行政院國家科學委員會補助專題研究計畫成果報告

液態鎵熱力學及結構之研究(2/2)

A study on structure and thermodynamics of liquid Ga (2/2)

計畫類別：個別型計畫
計畫編號：NSC 97－2112－M－009－0005－MY2
執行期間： 97 年 8 月 1 日 至 99 年 7 月 31 日

執行機構及系所：交通大學物理研究所

計畫主持人：吳天鳴
共同主持人：
計畫參與人員：蔡昆憲

成果報告類型(依經費核定清單規定繳交)： 完整報告

本計畫除繳交成果報告外，另須繳交以下出國心得報告：
出席國際學術會議心得報告

處理方式：得立即公開查詢

中 華 民 國 99 年 10 月 18 日

國科會補助專題研究計畫成果報告自評表

請就研究內容與原計畫相符程度、達成預期目標情況、研究成果之學術或應用價值（簡要敘述成果所代表之意義、價值、影響或進一步發展之可能性）、是否適合在學術期刊發表或申請專利、主要發現或其他有關價值等，作一綜合評估。

1. 請就研究內容與原計畫相符程度、達成預期目標情況作一綜合評估 ■達成目標
2. 研究成果在學術期刊發表或申請專利等情形： 論文：■已發表 □未發表之文稿 □撰寫中 □無
3. 請依學術成就、技術創新、社會影響等方面，評估研究成果之學術或應用價值（簡要敘述成果所代表之意義、價值、影響或進一步發展之可能性）（以500 字為限） 液態鎵以結構奇異聞名，主要是表現在靜態結構因子主峰右側有一肩膀狀的突出部份。其結構來源成因，一直是實驗觀察到至今約半世紀未解釋完全的問題。在過去多用共價雙原子分子(dimer)解釋。然而，我們用一液態鎵位能模型，發現幾點用雙原子分子解釋矛盾之處。根據我們的模型與結果，此奇異結構並非由雙原子分子所造成，而是由鎵原子短程的軟排斥力及長程的價電子振盪位能所造成。我們的結論已發表於國際期刊上。

中文摘要

用從第一原理所得到的液態鎵位能模型，我們研討液態鎵溫度在熔點上一些的微觀結構與熱力學性質。在此模型中，兩鎵原子間的作用力包括短程的排斥力與長程的 Friedel 振盪位能，而此短程的斥力是非常“軟”的。此模型的 excess Helmholtz 自由能及 excess entropy 均利用硬球微擾理論及熱力學積分公式計算。因所得計算結果與實驗值非常接近，我們結論此位能模型能的熱力學性質非常接近真實的液態鎵，此部分已發表在 Journal of Chemical Physics 129, 024503 (2008) 。

溫度在熔點上一些時，液態鎵以結構奇異聞名，主要是表現在靜態結構因子主峰右側有一肩膀狀的突出部份。此奇異結構實驗觀察到至今約半世紀，然其來源成因一直是未解釋完全的爭議問題。在過去多用共價雙原子分子(dimer)解釋，認為此共價雙原子分子是固態鎵剛熔化後的殘留物。然而，根據我們的位能模型與結果，我們質疑這樣的解釋。我們發現此奇異結構是來自於一些在奈米尺度的中程秩序結構，而當鎵原子間只有短程的排斥力時，此奇異結構將不會出現。我們的結果已發表於 Journal of Chemical Physics, 132, 034502 (2010)。

為要近一步了解 Friedel 振盪位能對液態鎵熱力學性質與微觀結構的供獻，我們比較此位能模型有 Friedel 振盪位能和沒有時的 excess entropy，而比較顯示 Friedel 振盪位能會降低液態鎵的 excess entropy。此結論與我們所提的液態鎵結構出現中程秩序結構的解釋相符合。此部份的結論將發表在 Computer Physics Communications。

關鍵詞： 液態鎵、硬球微擾理論、菲德爾振盪位能、中程秩序結構。

英文摘要

In terms of a model potential derived from the first-principles theory, we have studied the structure and thermodynamics of liquid Ga at temperatures just above the melting point. The pair potential of this model includes a soft repulsive core and the long-range Friedel oscillations. The excess Helmholtz free energy and excess entropy of this model are calculated by both the hard-sphere (HS) perturbation theory, which has been generalized for the fluids with very soft repulsive cores, and the thermodynamic integration, which is recognized as an exact theory in thermodynamics. In this part, with calculated results very close to the experimental data, we conclude that our model well describes the thermodynamics of liquid Ga and our results are published in Journal of Chemical Physics **129**, 024503 (2008).

Liquid Ga is famous for anomalous structures, characterized by a shoulder on the high-q side of the first peak in static structure factor at temperatures just above the melting point. The high-q shoulder has been observed for over fifty years; however, its interpretation is still in dispute. One interpretation usually adopted in the past is that the anomalous structures are resulted from the covalent dimers, the remnants after the solid Ga melts just above the melting point. However, with our model, which also reproduces the structural and dynamics properties of liquid Ga, including the high-q shoulder in the static structure factor, we question this interpretation. We find that the anomalous shoulder structures are resulted from some medium-range order, which is the interplay of the soft repulsive core and the Friedel oscillations within a range of nano scale, and would not appear in the case that only the soft repulsive core presents. Our conclusions in this part have been published in Journal of Chemical Physics **132**, 034502 (2010).

To further investigate the roles of the Firedel osicallations in the thermodynamic properties of liquid Ga, we have compared the excess entropies of the models with and without the Friedel oscillations and the comparison indicates that the Friedel oscillations cause a decrease in the excess entropy of liquid Ga, which is consistent with our picture for the presence of some medium-range order. This conclusion will be appeared in Computer Physics Communications.

Key Wards: Liquid Ga, Hard-spere perturbation theory, Friedel oscillations, Medium-range order.

國科會補助專題研究計畫項下出席國際學術會議心得報告

日期：99 年 7 月 30 日

計畫編號	NSC 97－2112－M－009－0005－MY2		
計畫名稱	液態鎵熱力學及結構之研究(2/2)		
出國人員 姓名	吳天鳴	服務機構 及職稱	交通大學物理研究所 教授
會議時間 (I) (II)	99 年 7 月 12 日至 99 年 7 月 16 日 99 年 7 月 19 日至 99 年 7 月 23 日	會議地點 (I) (II)	Hong-Kong, China Cairns, Australia
會議名稱 (I) (II)	(中文)香港統計物理會議 (英文) StatPhysHK: Complexity, Computation, Information (中文) 第二十四屆國際統計物理會議 (英文) The 24th International Conference on Statistical Physics		
發表論文 題目(I) 發表論文 題目(II)	(中文) 在一液態鎵模型內結構及(火商)之異常 (英文) Anomaly in Structures and Entropy of a Model for Liquid Ga (中文) 振動模在流動邊界的多重碎形 (英文) Multifractality of vibrational modes at mobility edge		

本人於今年(2010)七月十二日至十六日至香港出席由香港浸信會大學(Hong Kong Baptist University)所舉辦 StatPhysHK, Complexity, Computation, Information 的 Satellie 國際會議。此會議基本上有兩個主題: (A) 統計物理在生物系統之應用(Application of statistical physics in biology systems) 及 (B) 玻璃相變 (Glass transition). 其會議摘要可於下面網址查詢

http://www.hkbu.edu.hk/~statphys

參加的人數大約在二百人以上，主要來自歐洲、美國、日本、中國大陸、台灣與香港本

地的專家學者。會議中充滿學術討論的氣氛，包括研究方法、理論、實驗與電腦模擬。除了學術討論的氣氛，由會議規劃的細密可見其組織及用心，這也是參加此會議的收穫與心得。

本人在此會議中報告的論文(GD03)題目與摘要如下:

Anomaly in Structures and Entropy of a Model for Liquid Ga

The origin of high-q shoulder in the static structure factor of liquid Ga has been a long-standing problem. By simulating a model of interatomic pair potential, possessing a soft repulsive core and the Friedel oscillations, the anomalous structures and dynamical properties of liquid Ga just above the melting point have been reproduced. Dimers with bond lengths near that of the covalent bonds in Ga crystal are indeed found in our simulation. However, the high-q shoulder in the static structure factor is associated with interdimer pairs rather than the dimers themselves. By comparing the structures of the model in full range with those of the repulsive core only, we evidence that the high-q shoulder is associated with some medium-range order caused by Freidel oscillations within a nanoscale. The excess entropies of the two models are also examined. Our results indicate that the Friedel oscillations give rise to a decrease in the excess entropy, which is attributed to the medium-range order.

於香港會議之後，本人既前往澳洲凱恩斯(Cairns, Australia)參加第二十四屆國際統計物理會議 (International Conference on Statistical Physics). 此次會議日期是七月十九日到二十三日，由 The University of Queensland Australia 所舉辦.會議的網址如下

http://www.statphys.org.au/

會議的主題包括統計物理各方面

Topic 1	General aspects of statistical physics: phase transitions, critical phenomena, thermodynamics, networks and graphs, etc.
Topic 2	Mathematical aspects: rigorous results, exact solutions, matrix models, SLE, combinatorics etc.

Topic 3	Nonequilibrium processes: driven systems, transport theory, relaxation phenomena, random processes, fluctuations, large deviations etc.
Topic 4	Quantum systems: strongly correlated electrons, cold atoms, graphene, soft quantum matter, mesoscopic quantum phenomena, fractional quantum Hall effect, low dimensional quantum field theory, quantum phase transitions, quantum information and entanglement, etc.
Topic 5	Fluids and soft matter: molecular and ionic fluids, metastable liquids, polymers, gels, liquid crystals, microemulsions, foams, membranes, colloids, granular materials, etc.
Topic 6	Surfaces and Interfacial phenomena: growth processes, wetting, surface effects, films, confined systems, etc.
Topic 7	Non-linear phenomena: dynamical systems, pattern formation, hydrodynamic instabilities, turbulence, chemical reactions, etc.
Topic 8	Disordered and glassy systems: percolation, spin glasses, structural glasses, jamming, glass transition, algorithmic problems, etc.
Topic 9	Biological physics: molecular motors, dynamics at the scale of the cell, spatio-temporal organization in biological systems, biological membranes, biopolymer folding, etc.
Topic 10	Statistical modeling of biological data: genomics, biological networks, evolution models, etc.
Topic 11	Interdisciplinary topics in statistical physics: applied networks, econophysics, social phenomena, information theory, traffic flow, etc.

本人在此會議中報告的論文題目與摘要如下：

Multifractality of vibrational modes at mobility edge

Since Anderson’s pioneering work on the electron localization due to disorder, the localization-delocalization transition, also named as mobility edge (ME), has been a fundamentally important subject for over fifty years and a great impact on modern physics. At a ME, the wave phenomena exhibit multifractal behaviour, which indicates the self-similarity of the phenomena on all length scale. Recently, the multifractality of vibrational waves has been evidenced by the ultrasound on the 3-D elastic network of Al beads. In this work, we investigate the multifractals at the MEs in the instantaneous-normal-mode (INM) spectrum of a simple fluid; the INMs are referred to the eigenmodes of the Hessian matrices of the fluid configurations. In

terms of the level spacing (LS) statistics and the theory of finite size scaling, two MEs are found in the INM spectrum, one with positive eigenvalue and the other with negative eigenvalue. The locations of the two MEs are also confirmed by the multifractal analysis. Within numerical errors, the critical exponent and the nearest-neighbour LS distribution at each ME are in a good agreement with those of the 3-D Anderson model (AM). By comparing the singularity spectrum of the INMs at the MEs with that of the AM, we show that the behaviour of the multifractality at the ME is universal.

此次參加兩個統計物理方面的國際會議，學習和收穫豐富，本人非常感謝國科會經費的補助。

Hard-sphere perturbation theory for a model of liquid Ga

K. H. Tsai[1] and Ten-Ming Wu[2,a)]
[1]*Department of Electrophysics, National Chiao-Tung University, HsinChu, Taiwan 300, Republic of China*
[2]*Institute of Physics, National Chiao-Tung University, HsinChu, Taiwan 300, Republic of China*

(Received 22 April 2008; accepted 30 May 2008; published online 8 July 2008)

Investigating thermodynamic properties of a model for liquid Ga, we have extended the application of the hard-sphere (HS) perturbation theory to an interatomic pair potential that possesses a soft repulsive core and a long-range oscillatory part. The model is interesting for displaying a discontinuous jump on the main-peak position of the radial distribution function at some critical density. At densities less than this critical value, the effective HS diameter of the model, estimated by the variational HS perturbation theory, has a substantial reduction with increasing density. Thus, the density dependence of the packing fraction of the HS reference fluid has an anomalous behavior, with a negative slope, within a density region below the critical density. By adding a correction term originally proposed by Mon to remedy the inherent deficiency of the HS perturbation theory, the extended Mansoori–Canfield/Rasaiah–Stell theory [J. Chem. Phys. **120**, 4844 (2004)] very accurately predicts the Helmholtz free energy and entropy of the model, including an excess entropy anomaly. Almost occurring in the same density region, the excess entropy anomaly is found to be associated with the anomalous packing faction of the HS fluid. © *2008 American Institute of Physics*. [DOI: 10.1063/1.2948950]

I. INTRODUCTION

A general realization about simple liquids is that the liquid structure is primarily determined by the repulsive core of particles, while the attractions between particles determine the cohesion of the liquid.[1] Since the repulsions and attractions in a liquid play different roles in thermodynamics of the liquid, the two portions of interatomic interactions are individually approximated with different strategies. The structure of a liquid can be described by a reference fluid with the repulsive core only, whereas the attractions are treated as a perturbation. This forms the central theme of thermodynamic perturbation theory, which has played an important role in the development of statistical mechanism for simple liquids.[2,3] Some refinements of the theory progress recently, with an aim of applications in soft condensed systems.[4–9]

Owing to the benefit of available analytical expressions of the hard-sphere (HS) fluid in calculating thermodynamic and structural properties, the reference fluid is further approximated to be a HS one with the HS diameter determined by requiring that the two fluids are equivalent in some thermodynamic quantity. For example, in the Weeks–Chandler–Andersen (WCA) theory,[10–13] the HS diameter is determined by the equation of equal compressibility between the two fluids so that their free energies differ in the fourth order of the softness parameter, which is a measure for the difference between the repulsive core and the HS potential. Generally, the WCA theory is accurate for the Lennard-Jones (LJ) fluids at high densities. However, as the repulsive core is very soft, the softness parameter is so large that the inaccuracy of the WCA theory becomes serious. With a different choice for the HS diameter, Lado[14] gave some improvement in the prediction of the WCA theory. Alternatively, according to the Gibbs–Bogolubov inequality, Mansoori–Canfield[15] and Rasaiah–Stell[16] (MCRS) developed independently a variational approach, based on a HS reference system and the first-order perturbation. By treating the HS diameter as a variational parameter, this approach provides an upper bound of the Helmholtz free energy. As the repulsive core is softer than that of the LJ potential, the prediction of this variational approach is found to be more accurate than that of the WCA theory. This variational HS perturbation theory has been applied to calculate the structures and thermodynamics of liquid metals, which can be described by the effective pair potentials with very soft repulsive cores.[17–20]

Pointed out by Mon[21–23] in a few years ago, the inaccuracy of the HS perturbation theory is resulted from an inherent deficiency of the theory: A region in the phase space of a realistic fluid is forbidden by a HS fluid due to the singularity of the HS potential. To make up the deficiency of the HS perturbation theory, Mon proposed a correction term that should be added into the variational function to improve the accuracy of the variational approach. By testing the corrected variational function with the inversed-power fluids and a model of liquid Na,[24] the deficiency of the HS perturbation theory is accounted. Recently, including Mon's correction term in the two-body approximation, Ben-Amotz and Stell have extended the MCRS theory.[25] Different from other HS perturbation theories, this extended theory needs two effective HS diameters. The cavity distribution function of a HS fluid, which is in the correction term, is evaluated by the HS-diameter value determined by the Lado-WCA method; other HS-diameter parameters, appearing either explicitly or implicitly in the variational function, are still treated as the variational parameter. Also tested with the inversed-power

a)Author to whom correspondence should be addressed. Electronic mail: tmw@faculty.nctu.edu.tw.

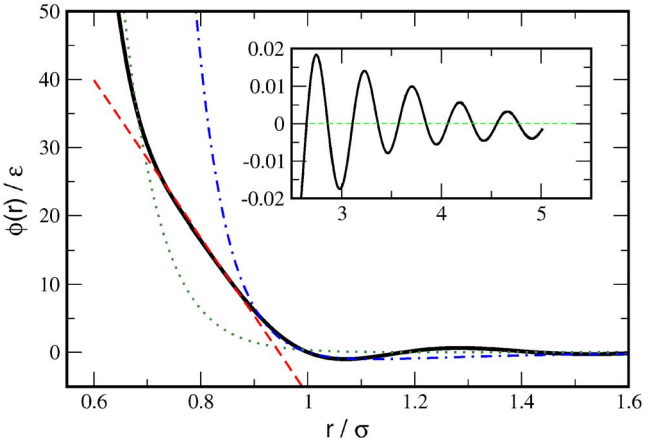

FIG. 1. (Color online) Interatomic pair potential $\phi(r)$ (solid line). The dot-dashed line is the LJ potential with the same ε and σ. The dashed line is a linear function $a_1(r/\sigma)+a_2$ with $a_1=-115\varepsilon$ and $a_2=109\varepsilon$; the dotted line is the function $c_1 \exp(-c_2 r/\sigma)(r/\sigma)^{c_3}$, where $c_1=4.42\times10^6\varepsilon$, $c_2=16.4$, and $c_3=1.5$. The inset shows the oscillatory part of $\phi(r)$ at large distances.

fluids, the extended-MCRS (E-MCRS) theory gives more accurate predictions than other first-order HS perturbation theories.

In terms of an interatomic pair potential generated by a first-principles pseudopotential theory,[26] the structural and dynamic properties of liquid Ga close to the triple point are well described, including the well-known shoulder in static structure factor and the anomaly in the linewidth function of dynamic structure factors at high wavevectors.[27] This interatomic pair potential is characterized by two features: a ledge-shape repulsive core and the long-range oscillations induced by conduction electrons. Although generated numerically, the interatomic pair potential is continuous and smooth, and the behavior of the repulsive core is generally like the two-scale Jagla potential,[28] which have been used to investigate the waterlike anomalies.[29–31] It is interesting to examine the accuracy of the HS perturbation theories mentioned above with this liquid-Ga model, by comparing their predictions with the simulation results. We also estimate the effective HS diameter of this model fluid by these perturbation theories and compare their density variations. We find that the E-MCRS theory gives extraordinarily accurate predictions on the thermodynamic properties of this model from low to high densities, including an excess entropy anomaly at intermediate densities. In the next section, we briefly outline the MCRS and E-MCRS theories. In Sec. III, our model is described and the conditions of our simulations are given. In Sec. IV, we present the calculated results. Our conclusions are given in Sec. V.

II. THEORETICAL BACKGROUND

The excess Helmholtz free energy A^{ex} of a fluid is defined as the difference between the total free energy of the fluid and that of an ideal gas at the same number density ρ and temperature T. A^{ex} is attributed to interactions between particles. Here, we give two methods for how A^{ex} is calculated. The first method is based on the HS perturbation theory and the second is evaluated by a thermodynamic integration of pressure.

Relative to a reference fluid of HSs with diameter σ_{HS} at the same temperature and number density, $\tilde{A}=A^{\mathrm{ex}}/Nk_BT$ of a fluid with N particles can be expressed as

$$\tilde{A} = \tilde{A}_{\mathrm{HS}} + \Delta\tilde{A}, \tag{1}$$

where $\tilde{A}_{\mathrm{HS}}=A^{\mathrm{ex}}_{\mathrm{HS}}/Nk_BT$ is the corresponding quantity of the HS fluid and $\Delta\tilde{A}$ is the difference. $\tilde{A}_{\mathrm{HS}}$ is well described by the Carnahan–Starling expression,[32]

$$\tilde{A}_{\mathrm{HS}} = \frac{\eta(4-3\eta)}{(1-\eta)^2}, \tag{2}$$

where $\eta=\pi\rho\sigma^3_{\mathrm{HS}}/6$ is the packing fraction of the HS fluid. In the MCRS theory,[15,16] $\Delta\tilde{A}$ of a fluid with a pair potential $\phi(r)$ is given as

$$\Delta\tilde{A} \approx 2\pi\rho\beta\int_{\sigma_{\mathrm{HS}}}^{\infty} g_{\mathrm{HS}}(r)\phi(r)r^2dr, \tag{3}$$

where $g_{\mathrm{HS}}(r)$ is the radial distribution function of the HS fluid and $\beta=(k_BT)^{-1}$. By treating σ_{HS} as a variational parameter, a measured value of $\tilde{A}$ is obtained by minimizing a sum of $\tilde{A}_{\mathrm{HS}}$ and $\Delta\tilde{A}$ given in Eqs. (2) and (3), respectively.

In principle, the entire configuration space Ω is accessible to a realistic fluid. Because of the singularity of a HS potential, part of Ω is not available to the HS fluid, which configuration space is denoted as Ω_{HS}. This is due to the excluded volume effect of the HS particles. Mon pointed out that due to the difference between Ω_{HS} and Ω a correction term that should be added into $\Delta\tilde{A}$ is formulated as[21–23]

$$\Delta_\eta = \frac{1}{N}\ln\left[\frac{\int_{\Omega_{\mathrm{HS}}} e^{-\beta\Phi}}{\int_{\Omega} e^{-\beta\Phi}}\right], \tag{4}$$

where Φ is the total interaction energy of the fluid of interest.

To the lowest order of fluid density, Ben-Amotz and Stell have shown that the correction term can be approximated to be[25]

$$\Delta_\eta = -2\pi\rho\int_0^{\sigma_{\mathrm{HS}}} g(r)r^2dr, \tag{5}$$

where $g(r)$ is the radial distribution function of the fluid with $\phi(r)$. As commonly used in the HS perturbation theory, $g(r)$ in the repulsive-core region is approximated as

$$g(r) = y_{\mathrm{HS}}(r)\exp(-\beta\phi(r)), \tag{6}$$

where $y_{\mathrm{HS}}(r)$ is the cavity distribution function of the HS reference fluid. By using this approximation, a new variational formula of $\Delta\tilde{A}$, refereed as the E-MCRS theory, is given as

$$\Delta\tilde{A} = 2\pi\rho\beta\int_{\sigma_{\mathrm{HS}}}^{\infty} g_{\mathrm{HS}}(r)\phi(r)r^2dr - 2\pi\rho\int_0^{\sigma_{\mathrm{HS}}} y_{\mathrm{HS}}(r)\exp(-\beta\phi(r))r^2dr. \tag{7}$$

It has been shown that the E-MCRS theory gives better predictions in thermodynamic properties of the inverse-power fluids than other first-order HS perturbation theories. How-

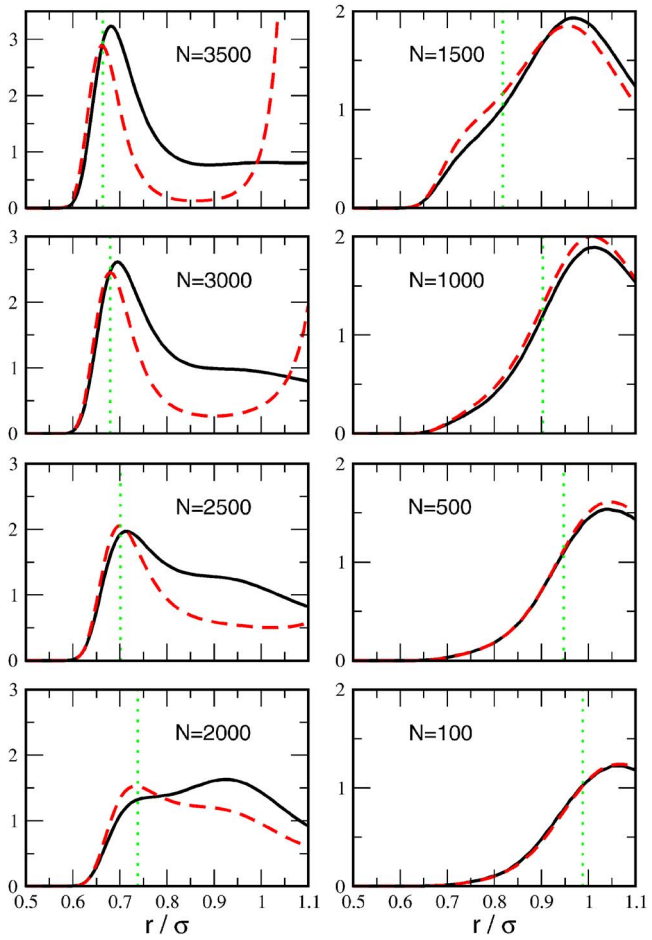

FIG. 2. (Color online) Radial distribution function of the model fluid at the indicated particle number. In each panel, the solid and dashed lines are, respectively, the simulation result and the approximation given by Eq. (6) with $y_{HS}(r)$ evaluated at the Lado-WCA value of σ_{HS}. The dotted line indicates the σ_{HS} value obtained by the E-MCRS theory.

ever, a notice should be given: The HS diameter for describing $y_{HS}(r)$ in the second integral is determined by the Lado-WCA method and may have a different value from that of the variational parameter σ_{HS}, which implicitly determines $g_{HS}(r)$ in the integrand of the first integral and appears explicitly in the lower and upper limits of the first and second integrals, respectively.

In thermodynamics, $\tilde{A}$ of a fluid at density ρ is related to the pressure $P(\rho')$ of the fluid at lower density ρ' via the following integration:[2]

$$\tilde{A} = \int_0^{\rho} \left(\frac{\beta P(\rho')}{\rho'} - 1 \right) \frac{d\rho'}{\rho'}. \tag{8}$$

$P(\rho')$ can be obtained via the pressure equation, in which two inputs are the radial distribution function of the fluid at density ρ' and the first derivative of the pair potential. With the radial distribution functions generated by computer simulation, $\tilde{A}$ obtained via the integration in Eq. (8) is recognized as the simulation results, which have no approximations in thermodynamics.

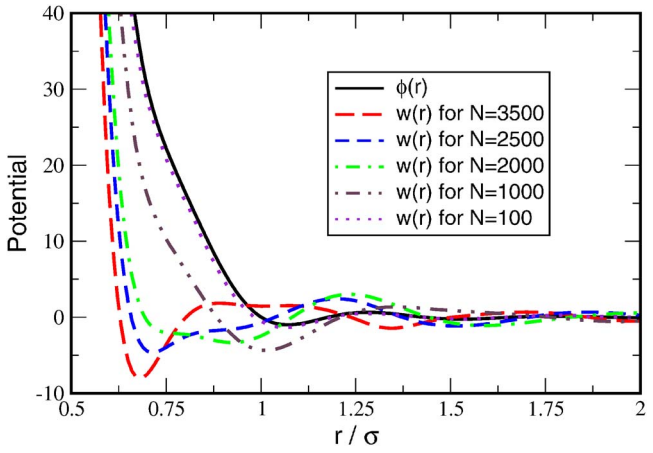

FIG. 3. (Color online) Potential of mean force $w(r)$ of the model fluid at $N=3500$ (dashed line), 2500 (short-dashed line), 2000 (dot-dashed line), 1000 (dot-dot-dashed line), and 100 (dotted line). The solid line is the interatomic pair potential $\phi(r)$. All potentials are scaled with ε and distance is scaled with σ.

III. MODEL OF LIQUID Ga AND SIMULATIONS

The interatomic pair potential $\phi(r)$ used in this paper is generated by a first-principles pseudopotential theory for liquid Ga at $T=323$ K.[26] Although the numerical data of $\phi(r)$ are generated at discrete points, the overall shape of $\phi(r)$, shown in Fig. 1, is continuous and smooth. Generally, $\phi(r)$ has a ledge-shape repulsive core and a long-range oscillatory part with a behavior following the Friedel oscillations.[27] Two parameters of $\phi(r)$ are ε, the depth of the main attractive well, and σ, which is the shortest distance at $\phi(r)=0$. The corresponding temperature of ε is about 47 K and $\sigma=4.04$ Å. The repulsive core of $\phi(r)$, denoted as $\phi_0(r)$, is the potential for r smaller than r_0, the position of the main attractive well, where r_0 is about 1.07σ. According to the behavior of the repulsive core, $\phi_0(r)$ can be roughly divided into three sections. As r is larger than 0.9σ, $\phi_0(r)$ with energy less than 6ε behaves like the repulsive core of the LJ potential with the same σ and ε.[33] In the intermediate region between 0.9σ and 0.7σ, the value of $\phi_0(r)$ varies from 6ε to 30ε and the shape of $\phi_0(r)$ becomes soft and has a ramplike behavior, with a reflection point around 0.8σ.[34] At r less than 0.7σ, $\phi_0(r)$ increases almost exponentially with decreasing distance so that the repulsive core changes to be extremely stiff.

With $\phi(r)$, we have carried out a series of molecular dynamics simulations at constant *NVE* ensemble by using a predictor-corrector algorithm[35] in a time step of 5.45 fs. In each simulation, the temperature is set to be 6.85ε, corresponding to $T=323$ K, the box size is fixed at 10.2σ, and the range of $\phi(r)$ is terminated at half of the box size. All quantities given in this paper are in units of σ, ε and the mass of Ga atom. The number of simulated particles starts at $N=3500$. Then, in each simulation for a new thermodynamic state, N is reduced by 100, with the lowest N being 100. At $N=3500$, the simulated system has a number density $\rho=0.05$ Å^{-3}, with a reduced density $\rho^* \equiv \rho\sigma^3$ equal to 3.305, which is close to that of liquid Ga at $T=323$ K and pressure of about 1 bar. At the simulated conditions of $N=3500$, the

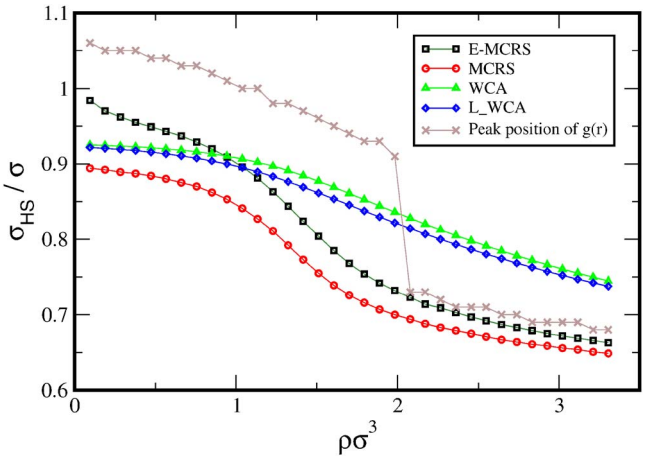

FIG. 4. (Color online) Effective HS diameter σ_{HS} as a function of density. σ_{HS} is estimated by various theories: WCA (triangles), Lado-WCA (diamonds), MCRS (circles), and E-MCRS (squares). The crosses stand for the main-peak position of $g(r)$. The symbols of each kind are connected by a line to guide the eye.

static and dynamic structure factors of the system reproduce well the experimentally observed structural and dynamic anomalies of liquid Ga at temperatures close to the melting point (T_m=303 K).[27]

The radial distribution functions of our simulated systems at some particle numbers are shown in Fig. 2. At N=3500, the main peak of the radial distribution function is located at 0.686σ, which is in the extremely stiff region of the repulsive core. As N is decreased, the main peak is lowered and shifts outwardly, while a shoulder near σ appears and then grows. Around N=2100, corresponding to $\rho^* \approx 2$, the roles of the main peak and the shoulder exchange: the main peak changes to occur near σ and the shoulder resides in the inner part of the repulsive core. As N keeps on decreasing, the inner shoulder gradually disappears, associated with a continuously growing main peak near σ as a compensation. As N is less than 1000, the number density of the system is rather low and the main peak moves toward the first attractive well, with a final position located at the minimum of the attractive well. A similar density variation of the radial distribution function is also observed for the one-scale and two-scale ramp potentials[31] introduced by Jagla[28] and the core-softened continuous potential with an attractive well.[36]

Another way to manifest the density effect on the radial distribution function of this model is to compare the potential of mean force, which is defined as $w(r)=-k_BT \ln g(r)$, with $\phi(r)$. $w(r)$ is the potential that gives the mean force acting on a particle in the fluid. In concept, the mean force between two neighboring particles in a dense fluid includes the direct force due to the interatomic pair potential and an effective force indirectly intermediated through other particles. In general, the indirect force depends on the fluid density, so the potential of mean force at high density can be quite different from the interatomic pair potential. For our model fluid, the variation of $w(r)$ with N is presented in Fig. 3. At N=3500, $w(r)$ has a deep attractive well at the first-peak position of $g(r)$; this attractive well is attributed to the compactness in the fluid at such a high density. As N is decreased, the depth of this attractive well gradually reduces, while a shoulder near σ appears. At some critical N, corresponding to a critical density, the roles of this attractive well and the shoulder in $w(r)$ switch with each other. As N is decreased further, the new attractive well in $w(r)$ continuously moves out, with its depth becoming deeper first and then attenuated to ε at final.

In the WCA theory,[11] the effective σ_{HS} of the model is determined by the solution of the following integral equation:

$$\int_0^{r_0} y_{HS}(r)\exp(-\beta\phi_0(r))r^2dr = \int_{\sigma_{HS}}^{r_0} y_{HS}(r)r^2dr. \quad (9)$$

This integral equation implies equal compressibility between the reference fluid with the repulsive core $\phi_0(r)$ and the fluid of HSs with diameter σ_{HS} at the same temperature and density. In the Lado-WCA method,[14] the effective HS diameter is given by the solution of a similar equation, by replacing $y_{HS}(r)$ in both integrands in Eq. (9) with $\partial y_{HS}(r)/\partial\sigma_{HS}$. To solve these equations efficiently, we have replaced $y_{HS}(r)$ and $\partial y_{HS}(r)/\partial\sigma_{HS}$ with their analytical expressions in the hard-fluid (HF) approximation,[37,38] which can be simply evaluated in terms of the packing fraction η of the HS fluid.

By using the discrete data of $\phi_0(r)$ and η evaluated at the simulated density, we have solved these equations to obtain the WCA and Lado-WCA values of HS diameter, and their density variations are shown in Fig. 4. For each method, our results are consistent with the general understanding that the effective HS diameter of a fluid is decreased with increasing the fluid density.[25] At each density, the HS diameters obtained by the two methods are close, with the WCA value larger. At high densities, both WCA and Lado-WCA σ_{HS} values are larger than the main-peak position of $g(r)$, which is located in the exponential region of the repulsive core. But, the HS diameters estimated at low densities becomes smaller than the main-peak position of $g(r)$, which has a sudden jump to a larger distance in the repulsive core with a LJ-type behavior around ρ^*=2. With the results shown in Fig. 2 for some particle numbers, we have examined the approximated $g(r)$ given in Eq. (6) for our model, with $y_{HS}(r)$ evaluated in the HF approximation at the Lado-WCA value of HS diameter. For our model at high densities, Eq. (6) is a good approximation of $g(r)$ for distances less than the main-peak position, while at low densities the validity of the approximation extends over the main peak of $g(r)$.

IV. THERMODYNAMIC PROPERTIES

Through the pressure equation with $g(r)$ generated by our simulations as an input, we have calculated the compressibility factor $Z \equiv \beta P(\rho)/\rho$ of our model and the results are shown by the symbols in Fig. 5. Theoretically, $Z(\rho)$ as a function of density can be expanded into a series with the leading term to be one.

$$Z(\rho) = 1 + b_2\rho + b_3\rho^2 + b_4\rho^3 + b_5\rho^4 + \cdots. \quad (10)$$

Here, b_i is the ith Virial coefficient, which is associated with $\phi(r)$ via some diagrams.[2] In the second Virial approximation, $Z(\rho)$ is approximated to be $1+b_2\rho$ and the calculation of b_2 is

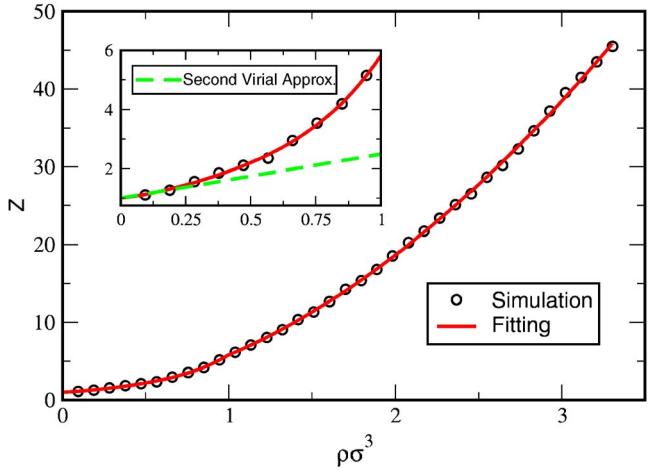

FIG. 5. (Color online) Compressibility factor, $Z=\beta P/\rho$, as a function of density. The circles are calculated by the pressure equation with the simulated $g(r)$ as an input. The solid line is the fitting function as described in the text with the fitting parameters given in Table I. The inset shows Z at low densities and the second Virial approximation (dashed line).

straightforward. Shown in the inset of Fig. 5 is the second Virial approximation of our model, which serves as a check for the accuracy of our calculations at low densities. In order to perform numerical integration in Eq. (8), we fit $Z(\rho)$ in Fig. 5 with the series in Eq. (10) truncated beyond the fourth order of ρ and treat the Virial coefficients as fitting parameters. To make the fitting accurate enough, the data of $Z(\rho)$ for ρ^* larger and smaller than 1 are fitted separately and the values of the fitting parameters are given in Table I. Although the fitting function has an unnoticed discontinuity at $\rho^*=1$, this discontinuity has little effect on the numerical values of $\tilde{A}$ at higher densities. By using the fitting function of $Z(\rho)$, we have done the integration in Eq. (8) and the calculated $\tilde{A}$ are indicated by the symbols in Fig. 7.

In the MCRS and E-MCRS theories, the variational $\tilde{A}$ is minimized with σ_{HS} as the only variational parameter. During the minimization process, $g_{\mathrm{HS}}(r)$ in the integral in Eqs. (3) and (7) is generated by the Verlet algorithm,[39] and $y_{\mathrm{HS}}(r)$ in the second integral in Eq. (7) is replaced by the analytical expression of the HF approximation[37,38] with the Lado-WCA σ_{HS} value. Shown in Fig. 6 are the variational curves of $\tilde{A}$ at some particle numbers. For each curve, the values of $\tilde{A}$ and the effective HS diameter at the minimum are determined numerically. Since the value of Mon's correction term decreases with increasing σ_{HS}, adding this correction term into the variational function causes the minimum of the variational curve shifting to a lower value of excess free energy and a larger value of effective HS diameter. Thus, for all thermodynamic states, the E-MCRS theory gives a better prediction on the excess Helmholtz free energy than the MCRS theory does, and the value of the HS diameter obtained by the E-MCRS theory is larger than that by the MCRS theory. These results are expected to be true for all kinds of fluid.[25]

TABLE I. The fitting coefficients of $Z(\rho)$ for $\rho^*<1$ and $\rho^*>1$. The data are given in unit of σ.

$Z(\rho)$	b_2	b_3	b_4	b_5
$\rho^*<1$	0.995	4.129	−4.969	4.670
$\rho^*>1$	−0.323	5.228	−0.523	0.055

In order to investigate the effect of the approximation in Eq. (6) on the values predicted by the E-MCRS theory, we also evaluate the variational $\tilde{A}$ with Mon's correction term Δ_η given in Eq. (5) with the simulated $g(r)$ used. As shown in Fig. 6, the corresponding variational curve of $\tilde{A}$ generally shifts upward relative to the one obtained by the E-MCRS theory, except that at very low densities the curves of the two methods are found to be almost the same. Therefore, our results lead to the conclusion that the approximation in Eq. (6) makes the prediction of the E-MCRS theory better.

In Fig. 4, the density variations of the effective HS diameters obtained by the MCRS and E-MCRS theories are compared to those obtained by the WCA and Lado-WCA theories. Similar as the results of the WCA and Lado-WCA theories, the σ_{HS} values estimated by the MCRS and E-MCRS theories also increase with decreasing density. For ρ^* larger than 2, the σ_{HS} values of the MCRS and E-MCRS theories are limited by the main-peak position of $g(r)$, with the density dependence of the E-MCRS value almost along the track of the peak position. For ρ^* less than 2 around which the main-peak position of $g(r)$ makes a jump to a larger value, the MCRS and E-MCRS values are apparently released from the restriction due to the main-peak position of $g(r)$ and ascend manifestly as ρ^* varies from 2 to 1. For ρ^* less than 1, the MCRS value becomes saturated roughly to 0.9σ as density approaches to zero, but the E-MCRS value continuously increases at very low densities and even passes over the values of the WCA and Lado-WCA theories.

The comparison of the excess Helmholtz free energies estimated by various HS perturbation theories is shown in Fig. 7. Apparently, the variational approaches do a better job than the WCA and Lado-WCA theories, which are only good for ρ^* less than 1. For all calculated densities, the predicted value of the E-MCRS theory is the one closest to the simulation data.

The excess entropy S^{ex} of a realistic fluid is defined as the difference between the entropy of the fluid and that of an ideal gas at the same density and temperature. In thermodynamics,

$$S^{\mathrm{ex}} = -(\partial A^{\mathrm{ex}}/\partial T)_{N,V}. \tag{11}$$

$\tilde{S}$ is defined as S^{ex}/Nk_B. In the MCRS theory, the excess entropy $\tilde{S}_{\mathrm{MCRS}}$ is equal to $-\tilde{A}_{\mathrm{HS}}$, which is the excess entropy of a HS fluid with the HS diameter of the MCRS value.[19] In the E-MCRS theory, Mon's correction term gives an extra contribution to $\tilde{S}$. In order to derive the extra contribution, we use the formula of Δ_η in Eq. (5), rather than the approximated one in Eq. (7). After substituting $g(r)=\exp(-\beta w(r))$ into Eq. (5), $\tilde{S}$ in the E-MCRS theory can be expressed as

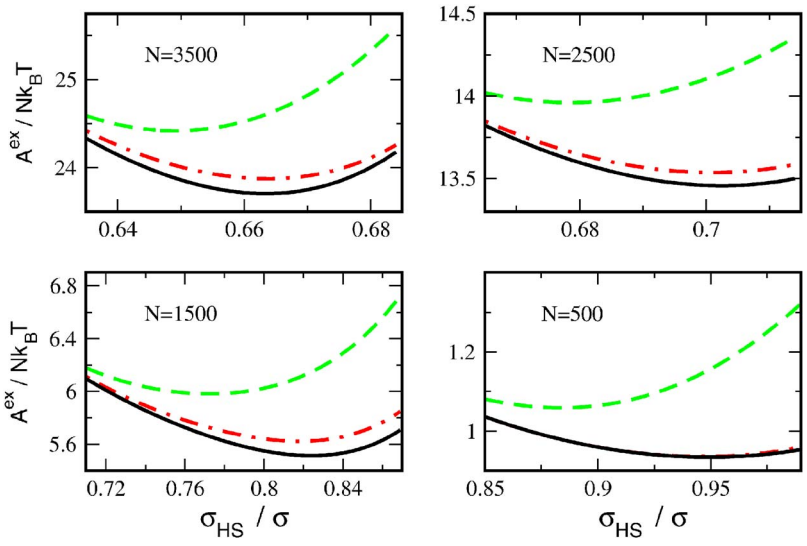

FIG. 6. (Color online) Variational $\tilde{A}$ as a function of σ_{HS} at the indicated particle number. In each panel, the solid and dashed lines are the E-MCRS and MCRS $\tilde{A}$, respectively. The dot-dashed line is the variational $\tilde{A}$ with Mon's correction term given in Eq. (5). For $N=500$, the solid and dot-dashed lines are almost the same.

$$\tilde{S}_{\mathrm{EMCRS}} = -\tilde{A}_{\mathrm{HS}} + 2\pi\rho \int_0^{\sigma_{\mathrm{HS}}} g(r)[1+\beta w(r)]r^2 dr. \quad (12)$$

Here, the second term on the right-hand side is due to Mon's correction term. Then, after using the approximation in Eq. (6) for $g(r)$,

$$\tilde{S}_{\mathrm{EMCRS}} = -\tilde{A}_{\mathrm{HS}} + 2\pi\rho \int_0^{\sigma_{\mathrm{HS}}} y_{\mathrm{HS}}(r)\exp(-\beta\phi(r)) \times[1+\beta\phi(r)-\ln y_{\mathrm{HS}}(r)]r^2 dr. \quad (13)$$

To evaluate $\tilde{S}_{\mathrm{EMCRS}}$, the HS diameter is required in three places in the above equation: the packing fraction in $\tilde{A}_{\mathrm{HS}}$, the upper limit of the integral in the second term, and $y_{\mathrm{HS}}(r)$, which is approximated to be the analytical expression of the HF approximation.[37,38] Care must be taken for that the value of σ_{HS} in the first and second places should be the one obtained by the minimization of variational $\tilde{A}$ in the E-MCRS theory but the Lado-WCA value of σ_{HS} should be used in the third place. Also, we have calculated Eq. (12) in terms of the simulated $g(r)$ and $w(r)$, and no significant difference is found between the results calculated by Eqs. (12) and (13). Thus, for our model, the two equations give almost identical results.

On the other hand, $\tilde{S}$ can be evaluated by the difference between the excess internal energy $\tilde{U}$ and the $\tilde{A}$ obtained by Eq. (8). By using $\phi(r)$ and the simulated $g(r)$, the calculation of $\tilde{U}$ is straightforward[2] and the result of $\tilde{S}$ is shown by the symbols in Fig. 8. The value of $\tilde{S}$ at $\rho^*=3.305$ is estimated to be −4.10, which is reasonably comparable to the experimental value of −4.62 of the excess entropy of liquid Ga at a higher temperature.[19] At low densities, $\tilde{S}$ decreases almost linearly with density; this decrease arises from the excluded volume effect due to the repulsive core of $\phi(r)$. Intriguingly, in the intermediate range of density, roughly from $\rho^*=1.4$ to 1.8, the density curve of $\tilde{S}$ has an anomalous behavior, which has a positive slope of a small value. Beyond this anomalous region, $\tilde{S}$ decreases again in a slower rate with increasing density. Observed also in the two-scale ramp potential,[40] the

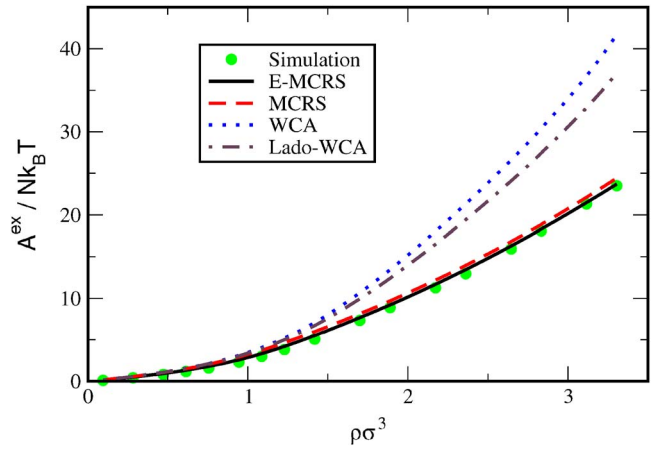

FIG. 7. (Color online) The excess Helmholtz free energy $\tilde{A}=A^{\mathrm{ex}}/Nk_BT$ predicted by the E-MCRS (solid line), MCRS (dash line), WCA (dotted line), and Lado-WCA (dot-dashed line) theories and the results calculated by thermodynamic integration in Eq. (8) (symbols).

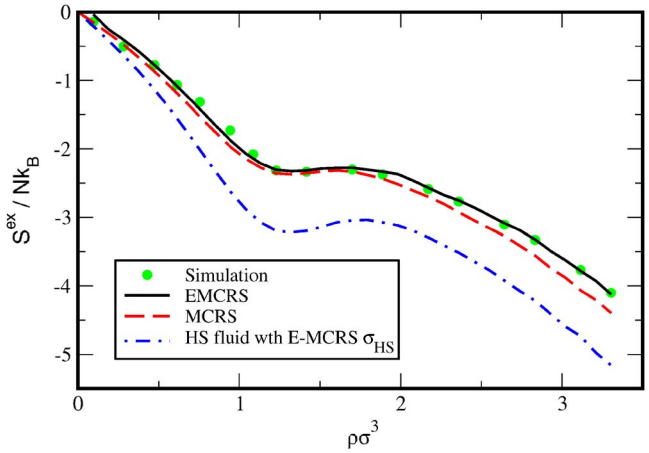

FIG. 8. (Color online) Density dependence of the excess entropy S^{ex}/Nk_B. The solid and dashed lines are the predictions of the E-MCRS and MCRS theories, respectively. The dot-dashed line is the excess entropy of the HS fluid with the HS diameter estimated by the E-MCRS theory. The symbols are the simulated results as described in the text.

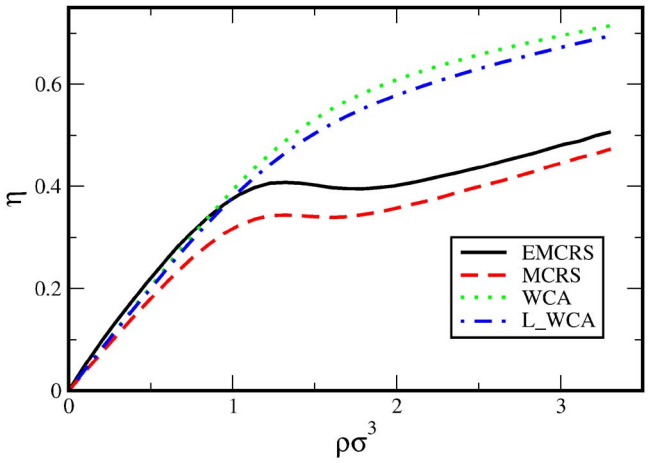

FIG. 9. (Color online) Density dependence of packing fraction η of the HS fluid with the E-MCRS (solid line), MCRS (dashed line), WCA (dotted line), and L-WCA (dot-dashed line) σ_{HS} values shown in Fig. 4.

anomalous behavior of $\tilde{S}$ is associated with the density anomaly, where the density increases with increasing temperature at constant pressure.[41]

For our model, the comparison between $\tilde{S}$ calculated by simulation and those obtained by the MCRS and E-MCRS theories is shown in Fig. 8; the three results of $\tilde{S}$ give similar density behavior. The predictions of the MCRS theory agree with the simulation results only at low densities and produce an excess entropy anomaly in a range shifting a little toward smaller density, but are deviated from the simulation data at densities beyond the anomalous region. The E-MCRS theory has a triumph over the MCRS theory for a perfect agreement with the simulation results in the entire range of density we have calculated. We also present the excess entropy of the HS fluid with the E-MCRS HS diameter, which shows a manifested anomaly with a larger positive slope. The absolute value of the excess entropy of this HS fluid is larger than that estimated by the E-MCRS theory. This implies that because part of the phase space is inaccessible by the HS fluid, in which the free volume of each particle is reduced, the difference between the entropy of the HS fluid and that of the ideal gas is, therefore, enhanced. Mon's correction makes a compensation for the excluded volume effect so that the predictions of the E-MCRS theory for all densities agree well with the simulation results. As indicated in Fig. 8, the larger the fluid density is, the more significant the compensation due to Mon's correction term. Thus, Mon's correction fundamentally improves the prediction of the HS variational approach for the excess entropy of a fluid.

To address the reason why the anomaly in $\tilde{S}$ predicted by the MCRS and E-MCRS theories occurs in our model, we have plotted in Fig. 9 the density dependence of the packing fractions of the reference HS fluids in various perturbation theories. In the WCA or the Lado-WCA theories, the packing faction η increases monotonically with the increase in density. At $\rho^*=3.3$, which is close to that of realistic liquid Ga, the η values estimated by the two theories are over 0.7, which is in the solid phase of a HS system. This indicates that because of the overestimation in the effective HS diameter, the reference HS fluids in the two theories are too much deviated from our model. On the other hand, with the σ_{HS} values estimated by the MCRS and E-MCRS theories, the density curve of the packing fraction apparently has a negative slope in the intermediate region, roughly from $\rho^*=1.3$ to 1.7, which corresponds to the substantial shrinkage in the size of the effective HS with increasing density, as shown in Fig. 4. Thus, the packing fraction of the HS fluid is reduced with increasing density in this density region. This anomaly in the packing fraction is the origin for the excess entropy anomaly predicted by the two theories. Beyond this anomalous region in packing fraction, the size of the effective HS is limited by the exponentially increasing repulsion in the inner core of the pair potential so that the packing fraction increases again with density at a smaller rate. At $\rho^*=3.3$, the packing fractions estimated by the MCRS and E-MCRS theories are, respectively, 0.473 and 0.5, which are in the fluid-solid coexistence region of the HS system, and the reference HS system is physically reasonable.

V. CONCLUSIONS

In terms of various HS perturbation theories, we have investigated thermodynamic behaviors of a model fluid, with which the structure and dynamic properties of liquid Ga close to the triple point are reproduced.[26,27] The interatomic pair potential of the model has two features: a ledge-shape repulsive core and a long-range oscillatory part. Somewhat like the two-scale ramp potential,[31,32] the repulsive core of the pair potential varies continuously from an exponential-decay inner core, through a ramplike intermediate region, to a LJ-type outer core. The model has been simulated at constant *NVE* conditions from low to high densities; at the highest density the simulated system corresponds to realistic liquid Ga at $T=323$ K. The radial distribution function of the model has an interesting variation with number density: At high density, the main peak of the radial distribution function is located in the inner region of the repulsive core with an exponential decay. At some critical density, the position of the main peak makes a discontinuous jump to the outer core of the LJ-type region. As the density is further decreased, the main peak moves toward the minimum of the first attractive well of the pair potential.

We have used the WCA, Lado-WCA, MCRS, and E-MCRS methods to estimate the effective HS diameter of the model. With the HS diameter estimated by the WCA or Lado-WCA method, the packing fraction of the HS system monotonically increases with density and, therefore, the packing fractions at high densities are over the freezing point of the HS system, which makes the WCA and Lado-WCA theories breakdown for our model at high densities. In the MCRS and E-MCRS theories, due to the structural change resulted from the discontinuous jump in the main-peak position of the radial distribution function, the estimated HS diameter is substantially reduced with increasing density, which renders the density curve of the packing fraction having a negative slope in a region of intermediate density. Beyond this negative-slope region, the packing faction of the

HS reference system increases again with density and has a physically reasonable value at high densities.

By including Mon's correction term to compensate the deficiency of the HS perturbation theory, the E-MCRS theory indeed gives better predictions than the MCRS theory does; the predictions of the E-MERS theory for the excess Helmohltz free energy and entropy agree well with the simulation results from low to high densities. The excess entropy of our model is found to have an anomalous behavior, which has a density function with a positive slope. This excess entropy anomaly also occurs in the two-scale ramp potential,[39] with which the waterlike thermodynamic properties are investigated recently.[30,31] The excess entropy anomaly in our model can be described by the E-MCRS and MCRS theories, and the anomaly is associated with the substantial reduction of the effective HS diameter estimated by the two variational theories. Our results indicate that the E-MCRS theory is superior to other first-order HS perturbation theories for investigating thermodynamics of core-softened potentials.

ACKNOWLEDGMENTS

T.M.W. would like to acknowledge financial support from the National Science Council of Taiwan, R. O. C. under Grant No. NSC 95-2112-M-009-027-MY2.

[1] C. Chandler, J. D. Weeks, and H. C. Andersen, Science **220**, 787 (1983).
[2] J. P. Hensen and I. R. McDonald, *Theory of Simple Liquids* (Academic, New York, 1986).
[3] J. A. Barker and D. Henderson, Rev. Mod. Phys. **48**, 587 (1976).
[4] D. Ben-Amotz and G. Stell, J. Phys. Chem. B **108**, 6877 (2004).
[5] F. O. Raineri, G. Stell, and D. Ben-Amotz, J. Phys.: Condens. Matter **16**, S4887 (2004).
[6] S. Zhou, Phys. Rev. E **74**, 031119 (2006).
[7] S. Zhou, J. Chem. Phys. **125**, 144518 (2006).
[8] S. Zhou, J. Phys. Chem. B **111**, 10736 (2007).
[9] A. B. Adib, Phys. Rev. E **75**, 061204 (2007).
[10] D. Chandler and J. D. Weeks, Phys. Rev. Lett. **25**, 149 (1970).
[11] J. D. Weeks, D. Chandler, and H. C. Andersen, J. Chem. Phys. **54**, 5237 (1971).
[12] H. C. Andersen, J. D. Weeks, and D. Chandler, Phys. Rev. A **4**, 1597 (1971).
[13] H. C. Andersen, D. Chandler, and J. D. Weeks, Adv. Chem. Phys. **34**, 105 (1976).
[14] F. Lado, Mol. Phys. **52**, 871 (1984).
[15] G. A. Mansoori and F. B. Canfield, J. Chem. Phys. **51**, 4958 (1969).
[16] J. Rasaiah and G. Stell, Mol. Phys. **18**, 249 (1970).
[17] D. Stroud and N. W. Ashcroft, Phys. Rev. B **5**, 371 (1972).
[18] J. Hafner, Phys. Rev. A **16**, 351 (1977).
[19] R. Kumaravadivel and R. Evans, J. Phys. C **9**, 3877 (1976).
[20] J. Hafner, *From Hamiltonians to Phase Diagrams* (Springer-Verlag, Berlin, 1987).
[21] K. K. Mon, J. Chem. Phys. **112**, 3245 (2000).
[22] K. K. Mon, J. Chem. Phys. **115**, 4766 (2001).
[23] K. K. Mon, J. Chem. Phys. **116**, 9392 (2002).
[24] K. K. Mon, Phys. Rev. E **63**, 061203 (2001).
[25] D. Ben-Amotz and G. Stell, J. Chem. Phys. **120**, 4844 (2004).
[26] S. F. Tsay and S. Wang, Phys. Rev. B **50**, 108 (1994).
[27] K. H. Tsai, T. M. Wu, S. F. Tsay, and T. J. Yang, J. Phys.: Condens. Matter **19**, 205141 (2007).
[28] E. A. Jagla, J. Chem. Phys. **111**, 8980 (1999).
[29] J. R. Errington and P. G. Debenedetti, Nature (London) **409**, 318 (2001).
[30] Z. Yan, S. V. Buldyrev, N. Giovambattista, and H. E. Stanley, Phys. Rev. Lett. **95**, 130604 (2005).
[31] Z. Yan, S. V. Buldyrev, N. Giovambattista, P. G. Debenedetti, and H. E. Stanley, Phys. Rev. E **73**, 051204 (2006).
[32] N. F. Carnahan and K. E. Starling, J. Chem. Phys. **51**, 635 (1969).
[33] T. M. Wu, S. F. Tsay, S. L. Chang, and W. J. Ma, Phys. Rev. B **64**, 064204 (2001).
[34] T. M. Wu, W. J. Ma, S. L. Chang, and S. F. Tsay, Physica B (Amsterdam) **316–317**, 606 (2002).
[35] A. Rahman, Phys. Rev. **136**, A405 (1964).
[36] A. B. de Oliveira, P. A. Netz, T. Colla, and M. C. Barbosa, J. Chem. Phys. **125**, 124503 (2006).
[37] L. E. S. de Souza and D. Ben-Amotz, Mol. Phys. **78**, 137 (1993).
[38] D. Ben-Amotz and G. Stell, J. Chem. Phys. **119**, 10777 (2003); **120**, 4994 (2004).
[39] L. Verlet and J. J. Weiss, Phys. Rev. A **5**, 939 (1972).
[40] J. R. Errington, T. M. Truskett, and J. Mittal, J. Chem. Phys. **125**, 244502 (2006).
[41] R. M. Lynden-Bell and P. G. Debenedetti, J. Phys. Chem. B **109**, 6527 (2005).

Revisiting anomalous structures in liquid Ga

K. H. Tsai,[1] Ten-Ming Wu,[1,a)] and Shiow-Fon Tsay[2]
[1]*Institute of Physics, National Chiao-Tung University, HsinChu, Taiwan 300, Republic of China*
[2]*Department of Physics, National Sun Yat-sen University, Kaohsiung, Taiwan 804, Republic of China*

(Received 2 November 2009; accepted 29 December 2009; published online 20 January 2010)

In terms of an interatomic pair potential, which well characterizes the dynamic properties of liquid Ga, we investigate again the origin of the well known high-q shoulder in the static structure factor of the liquid. Similar to the results of Gong's simulation at high temperature, dimers with extremely short bond lengths are indeed found in our model just above the melting point, but our results indicate that it is unlikely for the high-q shoulder to be produced by these dimers. Instead, based on our model, the high-q shoulder is resulted from some medium-range order, which is related to the structures beyond the first shell of the radial distribution function, caused by Friedel oscillations within a nanoscale range. © *2010 American Institute of Physics*. [doi:10.1063/1.3294565]

I. INTRODUCTION

Polyvalent liquid metals (Ga, Si, Ge, Sn, As, Sb, and Bi) are well known for anomalous structures, mainly characterized by a shoulder appearing on the high-q side of the first peak in the static structure factors of these liquids.[1,2] The origin of the shoulder structures has been a long-standing subtle problem in liquid metal physics and several scenarios have been proposed.[3–9] Using the interatomic pair potentials derived from the pseudopotential theory, which generally have a ledge-shaped repulsive core and the long-ranged Friedel oscillations, Hafner and co-workers reproduced the shoulder structures in liquid Ga, Ge, and Si,[5] and concluded that the peculiar static structure factor is determined by two characteristic lengths: the effective hard-sphere diameter required by sphere packing and the Friedel wavelength λ_F associated with the oscillatory part of the pair potential. The high-q shoulder is, therefore, predicted to occur near $2\pi/\lambda_F$.

Among these polyvalent elements, Ga shows uncommon properties, including low melting temperature (T_m=302 K), an increase in density upon melting, and complex solid-state phases under high pressure.[10] These properties are closely related to the existence of the covalent dimers, with a bond length of 2.44 Å, in solid Ga(α-Ga) at the ambient pressure.[11] Based on an *ab initio* simulation of Ga at T=1000 K, Gong *et al.*[7] found the existence of very short-lived covalent dimers, which were considered as the remnants as α-Ga melts and expected to increase in concentration at lower temperatures. They attributed the high-q shoulder in the static structure factor above T_m to the presence of these covalent dimers.

By classical molecular dynamics (MD) simulations with an interatomic pair potential generated by a first-principles pseudopotential theory, Tsay[12] reproduced not only the shoulder structures of liquid Ga, but also the naive structural variation in Ga as rapidly quenched from the liquid state to the supercooled and glassy states and then reheated. After analyzing the liquid and amorphous structures, Tsay[8] postulated that the shoulder structures in liquid Ga are primarily due to some four-atom clusters, which become predominated in the amorphous states and β-crystal. Thus, the origin of the high-q shoulder in the static structure factor of liquid Ga is still unclear and debated so far.

In the past decade, dynamics of liquid Ga has been intensively studied by inelastic scattering experiments.[13–17] The results of these experiments also provide information related to the structures of liquid Ga and play a role on examining the existing potential models used in simulations for mimicking the liquid. In Sec. II, we first investigate the validity of the pair potential $\phi(r)$ used in the simulations of Tsay by comparing the calculated dynamic quantities with several sets of inelastic scattering data, which include the dynamical structure factor $S(q,\omega)$, the dispersion relation, and the damping factor of collective excitations at low q as well as the linewidth of $S(q,\omega)$ at high q. Our results indicate that the model of Tsay, without any fitting parameters, is appropriate for describing the dynamics of liquid Ga. In Sec. III, we turn our attention to the structures produced by simulations with $\phi(r)$ at thermodynamic conditions of Ga at T =323 K. Dimers with bond lengths near 2.44 Å are indeed found in our simulation; however, we give several reasons to question the interpretation that the high-q shoulder in the static structure factor of liquid Ga is produced by the dimers themselves. On the other hand, by comparing the liquid structures generated with $\phi(r)$ truncated at different distances at the same NVT conditions, we find that the high-q shoulder is associated with some medium-range order, which is related to the structures beyond the first shell around a partilce.[18] The medium-range order, caused by the Friedel oscillations within a range of nanoscale, favors the formation of the four-atom clusters pointed out by Tsay. Our conclusions are given in Sec. IV.

II. COMPARISON OF OUR MODEL WITH THE EXPERIMENTAL RESULTS

Generated by the generalized energy independent nonlocal model pseudopotential (GEINMP) theory,[8] the inter-

a)Author to whom correspondence should be addressed. Electronic mail: tmw@faculty.nctu.edu.tw.

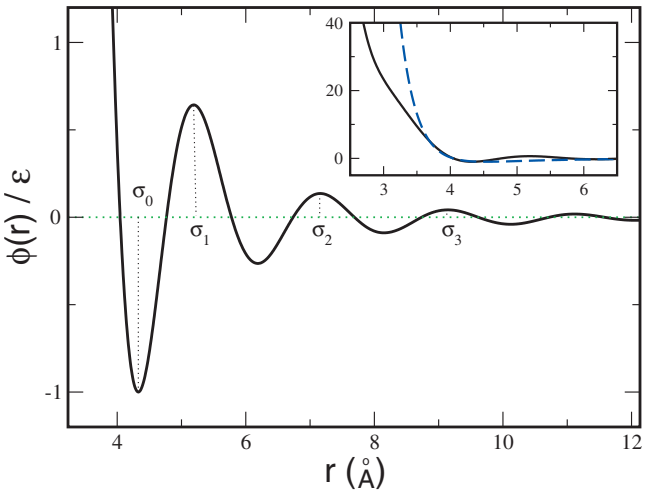

FIG. 1. Interatomic pair potential $\phi(r)$. ε is the depth of the first attractive well, corresponding to a temperature about 47 K. σ_0 is the location of the first minimum of $\phi(r)$. σ_1, σ_2, and σ_3 are the locations of the first, second, and third maxima of the oscillatory part, respectively. The inset shows the comparison between $\phi(r)$ (solid line) and the LJ potential (dashed line) with the same ε and the distance at the first zero of the potential.

atomic pair potential $\phi(r)$, shown in Fig. 1, has a soft repulsive core and an oscillatory part. In the oscillatory part, which has λ_F=1.93 Å, the minimum of the first attractive well is located at σ_0=4.32 Å, and the first, second, and third maxima of $\phi(r)$ are located at σ_1=5.17 Å, σ_2=7.15 Å, and σ_3=9.13 Å, respectively.

As with our previous works,[19,20] we perform MD simulations of 3500 particles interacting with $\phi(r)$ at T=323 K and number density ρ=0.05 Å^{-3}, which is close to the ion density of liquid Ga at this temperature and pressure of about 1 bar. In our simulation, the predictor-corrector algorithm is used and a time step is 5.45 fs. Under the periodic boundary conditions, particles are confined in a cubic box of length 41.25 Å and $\phi(r)$ is terminated at half of the box size.

Relative to $\phi(r)$, the first and second peaks of the radial distribution function $g(r)$ of the simulated liquid are located at 2.77 and 5.46 Å, which are distances well inside the repulsive core of $\phi(r)$ and slightly over the first maximum of Friedel oscillations, respectively. The calculated static structure factor $S(q)$, shown in Fig. 4, has the main peak at q_M =25.4 nm^{-1}, followed by a shoulder around 32.5 nm^{-1}, which exactly equals $2\pi/\lambda_F$.

In the following, we compare the dynamic properties calculated by the model of $\phi(r)$ to the experimental data.

A. Dynamic structure factors at low *q*

The dynamic structure factor $S_{\mathrm{MD}}(q,\omega)$ of $\phi(r)$ is obtained via a time Fourier transform of the intermediate scattering function generated by our simulation.[19] To compare to the experimental data of inelastic x-ray scattering (IXS), $S_{\mathrm{MD}}(q,\omega)$ is weighted by the detailed balance factor and then convoluted with the instrument resolution function, which has a width of 3.0 meV, used in the experiment.[13] The comparisons of our results with the experimental data of liquid Ga at T=315 K for three wave vectors are presented in Fig. 2, in which no fitting parameter is involved. Our model generally describes the dynamic structure factor of liquid Ga, except for a slight deviation at q=5.75 nm^{-1} due to the system size of our simulation.

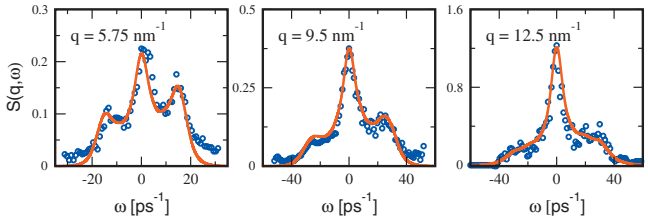

FIG. 2. Dynamic structure factor of liquid Ga. The solid lines are the results calculated by our model at T=323 K and the circles are the IXS data at T=315 K (Ref. 13).

B. Sound speed and the damping factor of collective excitations

Shown in Fig. 3 is the longitudinal current spectra $C_L(q,\omega)$ calculated by our model and analyzed with a damped harmonic oscillator (DHO) model,[21] which is expressed as

$$C_L(q,\omega) = \frac{A_q \omega_q \Gamma_q \omega}{(\omega^2 - \omega_q^2)^2 + (\Gamma_q \omega)^2}, \tag{1}$$

where the fitting parameters A_q, ω_q, and Γ_q are referred to the amplitude, energy, and damping of the longitudinal excitations at q, respectively. Obtained from the fits, ω_q and Γ_q at small q are found to be linear with q. In the insets of Fig. 3, the fit results of the dispersion relation and the damping fac-

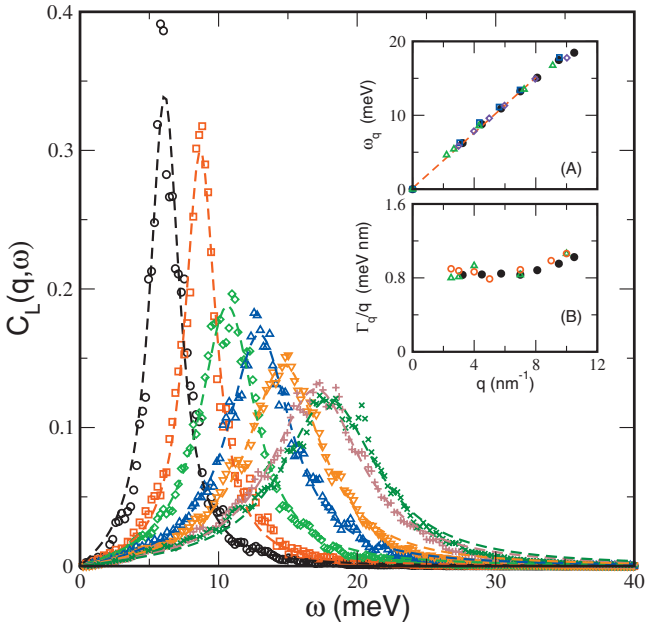

FIG. 3. Longitudinal current spectra $C_L(q,\omega)$ of our model at q =3.25 nm^{-1} (circles), 4.5 nm^{-1} (squares), 5.75 nm^{-1} (diamonds), 7.0 nm^{-1} (up triangles), 8.1 nm^{-1} (down triangles), 9.5 nm^{-1} (pluses), and 10.5 nm^{-1} (crosses). The dashed lines are the fits with the DHO model given in the text. The insets show (a) the excitation energy ω_q and (b) the damping factor Γ_q/q. The filled circles in (a) and (b) are the fit results of our model. In (a), the dashed line is the sound dispersion, and the open squares and diamonds are two sets of the IXS data at T=315 K (Ref. 13) and T=373 K (Ref. 17), respectively. The open triangles in (a) and (b) are the INS data at T =320 K and the open circles in (b) are the results of other model (Ref. 14).

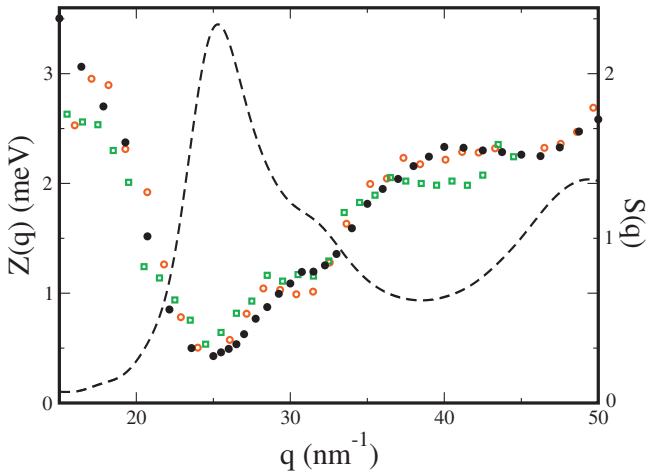

FIG. 4. Spectral linewidth $Z(q)$ of dynamic structure factor at high q. The filled circles are the results of our model. The open circles and squares are the data of IXS (Ref. 15) and QENS (Ref. 16) at $T=315$ K, respectively. The dashed line is the $S(q)$ of our model with a scale referred to the right axis.

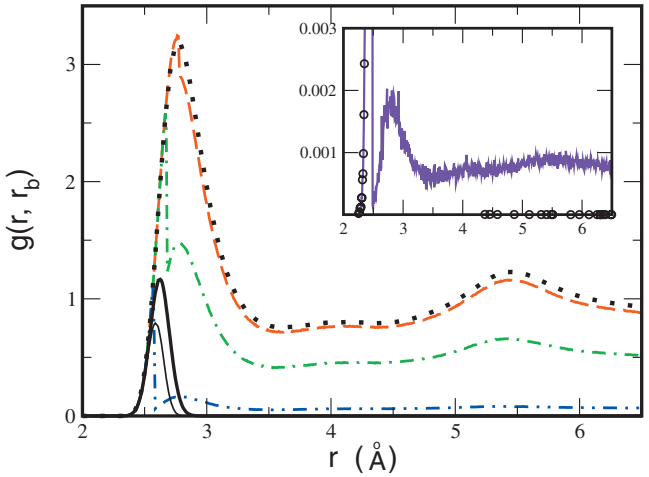

FIG. 5. Radial distribution functions of bonded atoms for $r_b=2.78$ Å (dashed line), 2.68 Å (dotted-dashed line), and 2.58 Å (dotted-dotted-dashed line) in the main panel and for $r_b=2.48$ Å (solid line) and 2.38 Å (open circles) in the inset. The dotted line is $g(r)$ of the liquid. The thick and thinner solid lines are the distributions of the NN and the MNN pairs in the liquid, respectively (Ref. 25).

tor Γ_q/q versus q are compared to the corresponding experimental data.[13,14,17] Through the low-q limit of the dispersion relation, the sound speed of our model is estimated to be 2860 cm/s, which is consistent with the adiabatic sound speed of liquid Ga just above T_m.[22] Also, the damping factor Γ_q/q of our model is in good agreement with those obtained by inelastic neutron scattering (INS) and the prediction of other model.[14]

C. Spectral linewidth of dynamic structure factor at high *q*

For the wave vectors in the kinetic regime, the sound waves in a liquid are strongly damped and the dynamic structure factor has only a single, Lorentzian-like central peak.[23] For q larger than 15 nm^{-1}, $S_{\mathrm{MD}}(q,\omega)$ of our model can be fitted with a single Lorentzian. Shown in Fig. 4, the linewidth of the fit Lorentzian $Z(q)$ as a function of q exhibits a minimum, which is the so-called de Gennes narrowing, very close to q_M.[24] In the experimental data of the spectral linewidth of dynamic structure factor, an anomaly is observed on the high-q side of the de Gennes narrowing; the anomaly is a second minimum by the IXS technique[15] but a shoulder by the quasielastic neutron scattering (QENS) technique.[16] In our data of $Z(q)$, we also observe a shoulder on the high-q side of the de Gennes narrowing. The shoulder in $Z(q)$ is almost at the same position of the high-q shoulder in $S(q)$, with the width of the shoulder somewhat narrower than the one observed in the QENS experiment.

According to the comparisons given above, we confirm that our model is appropriate for describing the structures and dynamic properties of liquid Ga just above T_m.

III. ORIGIN OF THE ANOMALOUS STRUCTURES

A. Are the anomalous structures due to the dimers?

In order to address whether the shoulder appearing in $S(q)$ of our model arises from the dimers as proposed by Gong *et al.*,[7] we defined the bonded atoms as those having at least one neighbor within a cutoff r_b. From the distribution of the nearest-neighbor (NN) pairs shown in Fig. 5, we find that the values of r_b for our model is roughly from 2.34 to 2.93 Å. Besides the atomic pairs with separations less than r_b, which are referred to dimers, the radial distribution function $g(r,r_b)$ of the bonded atoms also has contributions from the interdimer pairs which separations are larger than r_b.

At $r_b=2.38$ Å, as shown in Fig. 5, the contributions to $g(r,r_b)$ from these two kinds of atomic pairs are well separated because the bonded atoms are rare. The concentration of the dimers is quite low; in average, only one dimer is found in each configuration of 3500 particles. The dimers with such a short bond length are actually the mutual NN (MNN) pairs, which are two atoms with each other as NNs.[25] Due to their short separations, the repulsive interaction within each MNN pair is much stronger than those felt by other atomic pairs in the liquid and this strong repulsion makes the MNN pair survive only within a very short lifetime (less than 100 fs) during a collision. As r_b increases, the dimers are not necessarily the MNN pairs and some dimers are connected to form clusters, with a result on $g(r,r_b)$ that the distribution is no longer separated but has a sharp jump at r_b and the interdimer contribution generally reflects the behavior of $g(r)$. At $r_b=2.78$ Å, the similarity between $g(r,r_b)$ and $g(r)$ indicates that almost all of atoms in the simulation are the bonded atoms.

The structure factor $S(q,r_b)$ of the bonded atoms with a cutoff at r_b can be obtained via the formula

$$S(q,r_b)=1+4\pi\rho\int_0^\infty (g(r,r_b)-n_b)\frac{\sin(qr)}{qr}r^2dr, \qquad (2)$$

where $n_b=N_b/N$ is the percentage of the bonded atoms in the simulated system. Correspondingly, $S(q,r_b)$ can be separated into $S_d(q,r_b)$ and $\Delta S(q,r_b)$, which are the structure factor due to the dimers and the residue owing to the interdimer pairs, respectively.

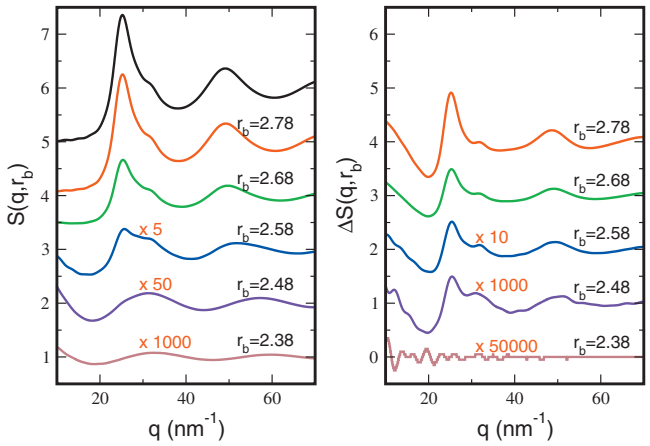

FIG. 6. Bonded-atoms structure factors $S(q,r_b)$ (left panel) and the residual structure factors $\Delta S(q,r_b)$ (right panel) for the r_b values in angstrom. Each curve is shifted upward by one unit from its lowered one. The top one in the left panel is $S(q)$ of the liquid. The values of the curves indicated with a red number have been amplified by the number.

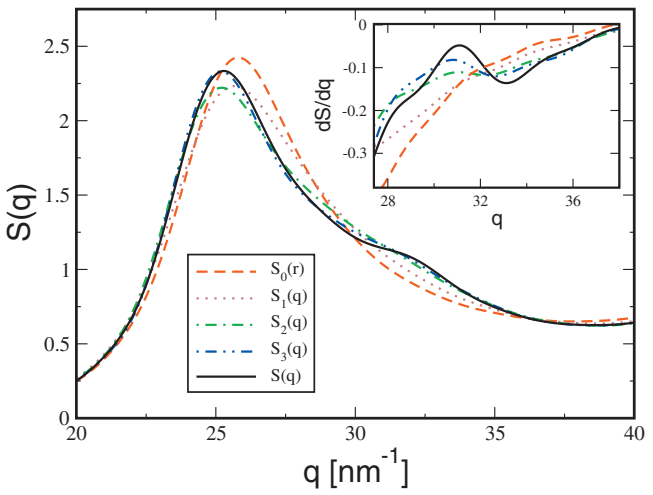

FIG. 7. Variation in static structure factor with the interaction range of $\phi(r)$. The solid line is for $S(q)$ of $\phi(r)$ and the dashed line is for $S_0(q)$ of $\phi_0(r)$ truncated at 4.32 Å. The dotted, dotted-dashed, and dotted-dotted-dashed lines are for $S_i(q)$ of $\phi_i(r)$ $(i=1,2,3)$, truncated at 5.17, 7.15, and 9.13 Å, respectively. The inset shows the first derivative of the corresponding static structure factors with respect to q.

$S(q,r_b)$ and $\Delta S(q,r_b)$ of our model are presented in Fig. 6 for several values of r_b. At $r_b=2.38$ Å, $S(q,r_b)$ is almost equivalent to $S_d(q,r_b)$ which oscillations can be approximated as $\sin(qr_b)/qr_b$.[24] As r_b increases, the behavior of $S(q,r_b)$ changes from the dimer structure factor to $S(q)$ of the liquid, with the main peak of $S(q)$ developing from a peak not appearing in $S_d(q,r_b)$ and the location of the high-q shoulder in $S(q)$ close to the maximum of $S_d(q,r_b)$ around $q\approx 32$ nm^{-1}. The variation in $S(q,r_b)$ with r_b agrees with Gong's results obtained by *ab initio* simulation at high temperature. However, the variations in $S_d(q,r_b)$ and $\Delta S(q,r_b)$ with r_b provide an evidence against the interpretation that the high-q shoulder originates from the dimers.

By increasing r_b up to 2.78 Å, $S_d(q,r_b)$ always behaves similarly, without much change in the oscillation but with a little increase in amplitude for more dimers are involved. On the contrary, the variation in $\Delta S(q,r_b)$ is quite dramatic. At $r_b=2.38$ Å, $\Delta S(q,r_b)$ is extremely small and fluctuated, since the interdimer pairs among the bonded atoms are rather rare. As r_b equals 2.48 Å, two peaks, with their positions very close to those of the main peak and the shoulder in $S(q)$, emerge in $\Delta S(q,r_b)$. By increasing r_b further, the two peaks are enhanced in value but their positions almost persist, and finally the shape of the two peaks is akin to the main peak and the shoulder in $S(q)$. This result gives an evidence that the high-q shoulder in $S(q)$ is associated with the interdimer pairs, rather than the dimers.

B. Medium-range order due to Friedel oscillations

To investigate the effective range of $\phi(r)$ to produce the shoulder in $S(q)$, we examine the variation in liquid structures with the interaction range of $\phi(r)$ from the repulsive core only to the full range. We have performed MD simulations at the same *NVT* conditions with the truncated pair potential $\phi_i(r)$ for $i=0,1,2,3$, which is obtained by truncating $\phi(r)$ at σ_i and shifting in energy by the value $\phi(\sigma_i)$ so that $\phi_i(r)$ has a finite range.[26] $\phi_0(r)$ is the repulsive core of $\phi(r)$. $\phi_1(r)$ contains the repulsive core and the first attractive well, with a depth corresponding to a temperature about 47 K. The ranges of $\phi_2(r)$ and $\phi_3(r)$ extend to include the first two and three attractive wells, respectively; the depths of these attractive wells decrease with increasing distance, as shown in Fig. 1. In the following, we present the static structure factors, the radial distribution functions and atomic bonded pairs (ABPs) (Ref. 8) of the fluids with the truncated $\phi_i(r)$.

1. Static structure factor

The static structure factors $S_i(q)$ of the fluids with $\phi_i(r)$ $(i=0,1,2,3)$ are shown in Fig. 7. $S_0(q)$ of the fluid with the repulsive core only is generally recovered back to the behavior of a hard-sphere fluid, with the first peak shifting to 25.7 nm^{-1} and increasing in magnitude. The essential difference between $S_0(q)$ and $S(q)$ is that there is no shoulder appearing on the high-q side of the first peak. By including the first attractive well in the pair potential, the first peak of $S_1(q)$, compared to $S_0(q)$, is lowered but has no significant change in position, while the values of $S_1(q)$ for q in the shoulder region, which is between 28 and 35 nm^{-1}, are elevated. The consequences of including the second attractive well are that the first peak of $S_2(q)$ shifts closer to that of $S(q)$ but has no change in magnitude and the values of $S_2(q)$ in the shoulder region are continuously elevated. The effect of extending the interaction range to include the third attractive well causes an increase in magnitude of the first peak and the appearance of a noticeable shoulder on the high-q side of the first peak; hence, $S_3(q)$ has a close resemblance to $S(q)$.

The appearance of the shoulder in the high-q region can be further identified by the derivative of $S_i(q)$ with respect to q, $dS_i(q)/dq$, which is shown in the inset of Fig. 7. In general, $dS_i(q)/dq$ on the high-q side of the first peak is negative and increases with q. A monotonic increase in $dS_i(q)/dq$ with q indicates that no shoulder appears in this region. Once a shoulder appears in $S_i(q)$, the behavior of $dS_i(q)/dq$ is

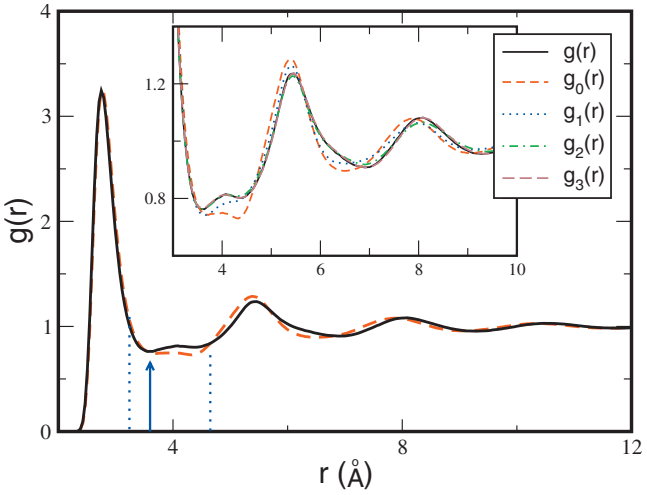

FIG. 8. Radial distribution functions of the liquid with $\phi(r)$ (solid line) and the fluid with $\phi_0(r)$ (dashed line). The two dashed lines indicate the distances of r_1 and r_2 in our evaluation for ΔN and the arrow indicates the bond length in the calculation of ABPs. The inset shows the variation in the second and third shells of the radial distribution function with the interaction range of $\phi(r)$.

distorted from a monotonic increase to the appearance of some extrema, where the slope of $dS_i(q)/dq$ is zero. The monotonic increase in $dS_0(q)/dq$ and $dS_1(q)/dq$ indicate that no shoulder appears in $S_0(q)$ or $S_1(q)$. $dS_2(q)/dq$ shows very weak extrema, signaling the emergence of a weak shoulder in $S_2(q)$. Evidenced by the clearly observed extrema in $dS_3(q)/dq$, the structures in the liquid of $\phi_3(r)$ are developed well enough to produce a shoulder in $S_3(q)$.

According to the results presented above, we conclude that the effective range of $\phi(r)$ for the full appearance of the shoulder structures should extend up to include the third attractive well; the effective range is, therefore, in a nanoscale.

2. Radial distribution function

In real space, the changes in the liquid structures with the range of pair potential are manifested in Fig. 8, which shows the comparison between $g(r)$ and the radial distribution functions $g_i(r)$ of the truncated $\phi_i(r)$. Clearly, all radial distribution functions possess almost the same first shell, indicating that dimers with extremely short bond lengths can be also found in the fluid with the repulsive core $\phi_0(r)$. Between the first and second peaks, all distribution functions have a small hump near 4 Å, which is close to the minimum of the first attractive well in $\phi(r)$. This small hump is also observed in the radial distribution function of liquid Ge.[27,28] In agreement with the case in static structure factor, the effective range in Friedel oscillations to make $g_i(r)$ saturated to $g(r)$ should include the first three attractive wells. As shown in the inset of Fig. 8, Friedel oscillations cause two effects on $g(r)$: pulling inward half a particle from the second shell to increase the small hump near 4 Å and pushing the second shell and the rest outward for compensation.[29] This gives an evidence that the high-q shoulder in $S(q)$ is associated with the structures beyond the first shell of $g(r)$, which possess some medium-range order in the liquid.[18]

3. Atomic bonded pairs

To manifest further the medium-range order due to Friedel oscillations, we calculate the averaged fractions of ABPs (Ref. 30) in the simulated liquids. It has been shown that as the system simulated with the pair potential generated by the GEINMP theory is quenched from liquid phase into amorphous solids or β crystal, the 1201-type ABPs become predominated. The 1201-type ABPs are clusters of four atoms, with two being a root pair and the other two being the common neighbors of the root pair within a bond length but the separation between the two common neighbors larger than the bond length.[12] Also, it is found that some large clusters formed with more 1201-type ABPs may produce a high-q shoulder in $S(q)$.[8] In this paper, we set the bond length to be 3.4 Å, which is close to the first-minimum distance of $g(r)$, so that the separation between the two common neighbors in the 1201-type ABPs is generally in the region of the small hump in $g(r)$. By comparing the calculated data given in Table I for the liquid of $\phi(r)$ and the fluid of $\phi_0(r)$, Friedel oscillations make the fraction of the 1201-type ABPs increase about 20%, which favor the occurrence of the high-q shoulder pointed out by Tsay.[8]

IV. CONCLUSIONS

In this paper, by classical MD simulation with an interatomic pair potential generated from the first-principles theory, we have reproduced the structural and dynamic properties of liquid Ga just above the melting temperature. Good agreement between the predictions of our model on dynamic properties and the experimental data suggests that our model is an appropriate one for describing liquid Ga.

Similar to the results of *ab initio* simulation reported by Gong *et al.*,[7] dimers with bond lengths comparable to that of the covalent molecules in solid α-Ga are indeed found in our model. However, we give several reasons to question the interpretation that the dimers are the origin of the high-q shoulder in the static structure factor of liquid Ga. First, the concentration of the dimers at temperatures just above melt-

TABLE I. Averaged fractions of ABPs N_{ijkl} in the fluids simulated with the full-range $\phi(r)$ and the truncated $\phi_i(r)$.

Pair potential	N_{1201}	N_{1211}	N_{1301}	N_{1311}	N_{1321}	N_{1421}	N_{1422}	N_{1431}
$\phi_0(r)$	0.156	0.048	0.114	0.253	0.067	0.052	0.105	0.081
$\phi_1(r)$	0.176	0.046	0.124	0.255	0.063	0.047	0.096	0.072
$\phi_2(r)$	0.191	0.046	0.133	0.252	0.059	0.042	0.091	0.064
$\phi_3(r)$	0.190	0.045	0.135	0.251	0.059	0.042	0.092	0.064
$\phi(r)$	0.188	0.045	0.134	0.251	0.059	0.042	0.093	0.065

ing point is quite low. Second, the extremely strong repulsion within a dimer makes the dimer unstable, surviving only for a very short lifetime during a collision. Besides these two, we provide evidences that the high-q shoulder is associated with the atomic pairs between the dimers, rather than the dimers themselves.

Our simulations indicate that Friedel oscillations produce a modulation on the local structures of particles, which are mainly determined by the soft repulsive core in our model. The modulation on the local structures gives rise to some stable medium-range order, which is related to the structures beyond the first shell of the radial distribution function. The high-q shoulder in the static structure factor is found to be associated with the medium-range order caused by Friedel oscillations. According to our model, the effective range of Friedel oscillations to produce the medium-range order should include, at least, the first three attractive wells, so that the effective range is in a nanoscale. Thus, our results are consistent with the picture given by Hafner *et al.*[5] that the shoulder structures are a result of the interplay between two length scales, characterizing the size of the repulsive core and the wavelength of Friedel oscillations.

The high-q shoulder in the static structure factor is a common feature to many polyvalent liquid metals. According to our study, the anomalous structures characterizing the high-q shoulder are quite complex, since a number of atoms, more than 20 estimated for liquid Ga, are involved. To manifest the anomalous structures, a picture of atomic structures in three-dimensional space is requested. This is challenging but important to fully understand the origin for the high-q shoulder of those polyvalent liquid metals and will be a future work.

ACKNOWLEDGMENTS

T. M. Wu and S. F. Tsay are indebted to the National Science Council of Taiwan, Republic of China for support under Grant No. NSC 97-2112-M-009-005-MY2 and NSC 98-2112-M-110-004-MY3, respectively.

[1] Y. Waseda, *The Structure of Non-Crystalline Materials, Liquids and Amorphous Solids* (McGraw-Hill, New York, 1980).
[2] J. Hafner, *From Hamiltonians to Phase Diagrams* (Springer-Verlag, Berlin, 1987).
[3] M. Silbert and W. H. Young, Phys. Lett. A **58**, 469 (1976).
[4] K. K. Mon, N. W. Ashcroft, and G. V. Chester, Phys. Rev. B **19**, 5103 (1979).
[5] J. Hafner and G. Kahl, J. Phys. F: Met. Phys. **14**, 2259 (1984).
[6] J. Hafner and W. Jank, Phys. Rev. B **42**, 11530 (1990).
[7] X. G. Gong, G. L. Chiarotti, M. Parrinello, and E. Tosatti, Europhys. Lett. **21**, 469 (1993).
[8] S. F. Tsay and S. Wang, Phys. Rev. B **50**, 108 (1994).
[9] L. E. Gonzalez, D. J. Gonzalez, and M. Silbert, Mol. Phys. **99**, 875 (2001).
[10] O. Degtyareva, M. I. McMahon, D. R. Allan, and R. J. Nelmes, Phys. Rev. Lett. **93**, 205502 (2004).
[11] X. G. Gong, G. L. Chiarotti, M. Parrinello, and E. Tosatti, Phys. Rev. B **43**, 14277 (1991).
[12] S. F. Tsay, Phys. Rev. B **50**, 103 (1994).
[13] T. Scopigno, A. Filipponi, M. Krisch, G. Monaco, G. Ruocco, and F. Sette, Phys. Rev. Lett. **89**, 255506 (2002).
[14] L. E. Bove, F. Formisano, F. Sacchetti, C. Petrillo, A. Ivanov, B. Dorner, and F. Barocchi, Phys. Rev. B **71**, 014207 (2005).
[15] T. Scopigno, R. Di Leonardo, L. Comez, A. Q. R. Baron, D. Fioretto, and G. Ruocco, Phys. Rev. Lett. **94**, 155301 (2005).
[16] F. J. Bermejo, I. Bustinduy, S. J. Levett, J. W. Taylor, R. Fernández-Perea, and C. Cabrillo, Phys. Rev. B **72**, 104103 (2005).
[17] S. Hosokawa, W. C. Pilgrim, H. Sinn, and E. E. Alp, J. Phys.: Condens. Matter **20**, 114107 (2008).
[18] S. R. Elliott, *Physics of Amorphous Materials*, 2nd ed. (Longman, Harlow, 1990).
[19] K. H. Tsai, T. M. Wu, S. F. Tsay, and T. J. Yang, J. Phys.: Condens. Matter **19**, 205141 (2007).
[20] K. H. Tsai and T. M. Wu, J. Chem. Phys. **129**, 024503 (2008).
[21] M. C. C. Ribeiro, M. Wilson, and P. A. Madden, J. Chem. Phys. **108**, 9027 (1998).
[22] M. Inui, S. Takeda, and T. Uechi, J. Phys. Soc. Jpn. **61**, 3203 (1992).
[23] T. Scopigno, G. Ruocco, and F. Sette, Rev. Mod. Phys. **77**, 881 (2005).
[24] J. P. Hansen and I. R. McDonald, *Theory of Simple Liquids* (Academic, New York, 2006).
[25] R. E. Larsen and R. M. Stratt, Chem. Phys. Lett. **297**, 211 (1998).
[26] N. Matsuda, K. Hoshino, and M. Watabe, J. Chem. Phys. **93**, 7350 (1990).
[27] V. Hugouvieux, E. Farhi, M. R. Johnson, F. Juranyi, P. Bourges, and W. Kob, Phys. Rev. B **75**, 104208 (2007).
[28] S. Munejiri, T. Masaki, T. Itami, F. Shimojo, and K. Hoshino, Phys. Rev. B **77**, 014206 (2008).
[29] Because of Friedel oscillations, the increase in the particle number around the small hump near 4 Å can be calculated by $\Delta N=4\pi\rho\int_{r_1}^{r_2}(g(r)-g_0(r))r^2dr$, where, as indicated in Fig. 8, r_1 is a distance in front of the small hump and r_2 is that close to the crossing point of $g(r)$ and $g_0(r)$ beyond the small hump. In our calculation, r_1 is set to be 3.24 Å and r_2 is 4.65 Å, and the value of ΔN is almost 0.5.
[30] J. D. Honeycutt and H. C. Andersen, J Phys. Chem. **91**, 4950 (1987). By following the nomenclature in the reference, the ABPs are characterized by four indices. The first index is 1 if the two atoms of a root pair are bonded. The second index represents the number of common neighbors, with each one bonded to the two atoms of the root pair. The third index gives the number of bonds among the common neighbors. These three indices are not sufficient to characterize a diagram uniquely. Therefore, a fourth index is required to specify a unique correspondence between the arrangement of atomic bonds and diagrams.

Computer Physics Communications ••• (••••) •••–•••

Contents lists available at ScienceDirect

Computer Physics Communications

www.elsevier.com/locate/cpc

Entropy of a model for liquid Ga: Contribution due to Friedel oscillations

K.H. Tsai *, Ten-Ming Wu

Institute of Physics, National Chiao-Tung University, HsinChu 300, Taiwan

ARTICLE INFO

Article history:
Received 1 March 2010
Received in revised form 8 July 2010
Accepted 12 July 2010
Available online xxxx

Keywords:
Liquid Ga
Friedel oscillations
Excess entropy

ABSTRACT

In terms of an interatomic pair potential, possessing a soft repulsive core and the long-range Friedel oscillations, we have recently reproduced the anomalous structures and dynamic properties of liquid Ga just above the melting point. In this paper, evaluating separately for the model and the corresponding repulsive core by numerical simulation and the hard-sphere perturbation theory, we investigate the contribution due to the Friedel oscillations to the excess entropy of the model fluid. For the two model fluids, the density variations of the pair-correlation and residual-multiparticle entropies are also presented.

1. Introduction

The structures of liquid Ga just above the melting point are well known for an anomalous shoulder on the high-q side of the first peak in the static structure factor. Recently, we have reproduced the anomalous structures with an interatomic pair potential $\phi(r)$ generated from a first-principles pseudopotential theory [1,2]. Besides the anomalous structures, the dynamic properties of liquid Ga, including dynamic structure factor, dispersion relation and the damping factor of collective excitations at low q as well as the linewidth of dynamic structure factor at high q, are also well described by this model. However, the anomalous structures are not produced by the repulsive core $\phi_0(r)$ of the model, but appear as the range of the pair potential extends up to including the third attractive well, within a range of nanoscale, in Friedel oscillations. Thus, we conclude that the anomalous structures are associated with some medium-range order due to the Friedel oscillations.

Motivated from the aforementioned results, we investigate in this paper the excess entropy contributed by the Friedel oscillations in $\phi(r)$. Arising from particle interactions, the excess entropy of a simple fluid is a thermodynamic quantity related to the degree of structural disorder of particles [3]. As far as we know, there are only few papers studying the role of the attractive particle interactions in the thermodynamic properties of polyvalent liquid metals [4]. For simple fluids, the structures are primarily determined by the repulsive core of particles and the attractions between particles act as a perturbation [5]. Based on this general picture, the contribution due to the Friedel oscillations can be obtained by the difference of the excess entropies of $\phi(r)$ and $\phi_0(r)$ at the same NVT conditions; the excess entropies are evaluated separately with both numerical simulation and the hard-sphere (HS) perturbation theory [6]. We also examine the density variations of the excess entropy and its pair-correlation and residual-multiparticle parts for the model fluid with $\phi(r)$ or $\phi_0(r)$ [7].

2. Model and the HS perturbation theory

Presented in [2,6], $\phi(r)$ is characterized by a ledge-shape repulsive core and a long-range oscillatory part, with the first zero of $\phi(r)$ at $\sigma = 4.04$ Å. The repulsive core $\phi_0(r)$ is obtained by truncating $\phi(r)$ at $\sigma_0 = 4.32$ Å, the location of the first minimum, and shifting upwardly by an amount of the first-attractive-well depth ϵ, which corresponds to a temperature about 47 K. Like the two-scale Jagla potential [8], $\phi_0(r)$ possesses an extremely stiff region following by a ramp.

We performed a series of molecular dynamics simulations for particles interacting with $\phi(r)$ in a cubic box of length $L = 41.21$ Å at $T = 323$ K [6]. The particle number N in the simulation starts at 3500 and, then, is reduced by 100 in each new simulation, down to the lowest $N = 100$. Two notices should be given here. First, at $N = 3500$, with $\rho\sigma^3 = 3.3$, the simulated system mimics the equilibrium state of liquid Ga at pressure of about 1 bar and $T = 323$ K; however, the systems at other particle numbers have nothing to do with real Ga. Secondly, both the radial distribution function $g(r)$ generated by the simulation and the compressibility factor $Z = PV/Nk_BT$, where pressure P is evaluated from the pressure equation with an input of $g(r)$, change smoothly with density [6], indicating that the simulated system does not undergo a gas–liquid phase transition as N is reduced. The temperature of our simulations is about seven times of ϵ so that the simulated systems are expected to be supercritical. Similarly, we also performed the simulations with the repulsive core $\phi_0(r)$ at the same NVT conditions.

* Corresponding author.
E-mail address: kht.ep94g@nctu.edu.tw (K.H. Tsai).

0010-4655/$ – see front matter
doi:10.1016/j.cpc.2010.07.014

Please cite this article in press as: K.H. Tsai, T.-M. Wu, Entropy of a model for liquid Ga: Contribution due to Friedel oscillations, Computer Physics Communications (2010), doi:10.1016/j.cpc.2010.07.014

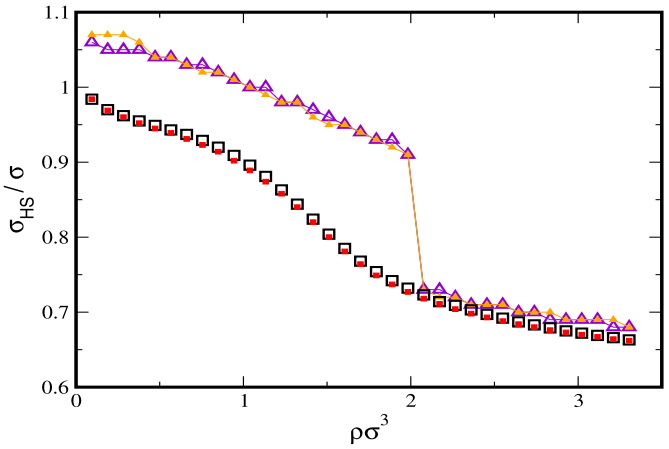

Fig. 1. Density variation of σ_{HS} estimated by the HS perturbation theory (squares) [9] and the main-peak position of $g(r)$ (triangles). $\rho = N/L^3$ is the number density. The large open symbols are for $\phi(r)$ and the small filled ones are for $\phi_0(r)$.

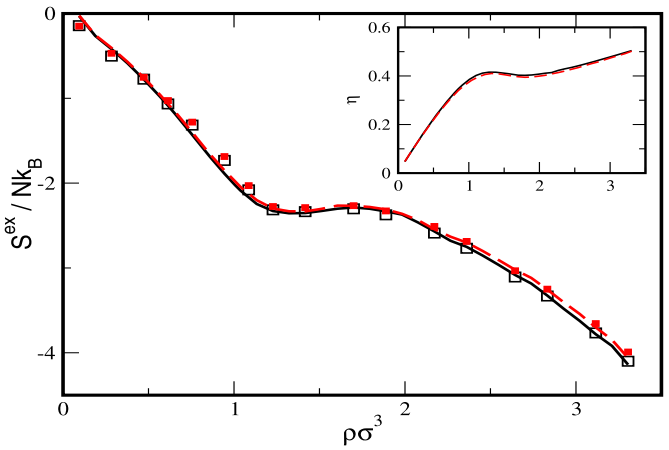

Fig. 2. Excess entropy S^{ex} as a function of density. The open and filled symbols are the simulation results for $\phi(r)$ and $\phi_0(r)$, respectively. The solid line is estimated by the HS perturbation theory for $\phi(r)$ and the dashed line is for $\phi_0(r)$. The inset shows the packing fraction η of the HS fluid with σ_{HS} shown in Fig. 1.

In thermodynamics, the excess entropy S^{ex} of a fluid is given as $(A^{ex} - U^{ex})/T$, where A^{ex} and U^{ex} are the excess Helmholtz free energy and the internal energy of the fluid, respectively [3]. The calculation for U^{ex} is straightforward and A^{ex} can be obtained by an integration on the density function of Z [6]. Without any approximation in thermodynamics, S^{ex} obtained in this method are considered as the simulation results. Alternatively, A^{ex} can be estimated by an HS perturbation theory, which accurately predicts the thermodynamic quantities of fluids with very soft repulsive-core potentials [9].

The HS perturbation theory estimates an effective diameter σ_{HS} of particles in a fluid. Shown in Fig. 1, the σ_{HS} values of the two models are almost the same for all densities, and so are the main-peak positions of $g(r)$. At low densities, the main-peak position of $g(r)$ is located around the first attractive well of $\phi(r)$. But, at high-enough densities, the jam in the system pushes more particles into the extremely stiff region of $\phi_0(r)$, which causes the main-peak position of $g(r)$ near $\rho\sigma^3 = 2$ a discontinuous jump to a smaller distance of r. At densities above $\rho\sigma^3 = 2$, the density dependence of σ_{HS} is almost along the track of the main-peak position of $g(r)$.

3. Excess entropy

For both models, a good agreement between the S^{ex} obtained by simulation and that estimated by the HS perturbation theory is shown in Fig. 2. Generally, S^{ex} of $\phi(r)$ is slightly less than that of $\phi_0(r)$ at high densities, indicating that the Friedel oscillations in $\phi(r)$ cause a small decrease in the excess entropy. At low densities, S^{ex} decreases almost linearly with density, due to the excluded volume effect of the repulsive core. More interestingly, the density function of S^{ex} shows an anomalous behavior, with a small positive slope in the intermediate region, and then changes back to decreasing at higher densities. The anomaly in the density function of S^{ex} also occurs to a model fluid with the two-scale Jagla potential [10]. Owing to the appearance of a similar anomaly in the packing-fraction curve of the HS fluid with σ_{HS}, the S^{ex} anomaly can be explained by the shrinkage of σ_{HS} at the intermediate densities shown in Fig. 1.

The difference in S^{ex} between the two models is too small to be noticeable. To manifest clearly the difference, we separate S^{ex} per particle into the pair-correlation entropy S_2 and the residual multiparticle entropy (RMPE) $\Delta S = S^{ex} - S_2$ [7], where S_2 is related to $g(r)$ via the equation

$$S_2 = -\frac{\rho k_B}{2}\int d\mathbf{r}\left[g(r)\ln g(r) - g(r) + 1\right]. \quad (1)$$

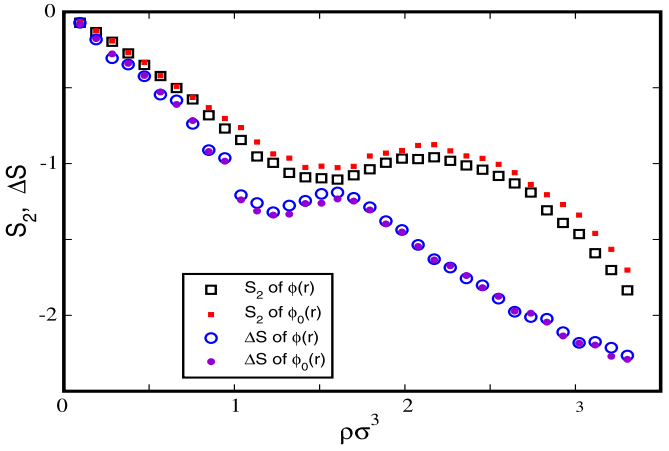

Fig. 3. Density dependence of pair-correlation entropy S_2 (squares) and RMPE ΔS (circles) in unit of k_B. The large open symbols are for $\phi(r)$ and the small filled ones are for $\phi_0(r)$.

S_2 is associated with the pair correlation in a fluid and ΔS is related to the three-particle and higher order correlations. The density variations of S_2 and ΔS for the two models are shown in Fig. 3. Evidenced by our data, ΔS of the two models are almost the same from low to high densities. S_2 of $\phi_0(r)$ is larger than that of $\phi(r)$, with a noticeable difference in Fig. 3. Thus, we conclude that the Friedel oscillations in $\phi(r)$ cause a decrease in S_2.

4. Conclusions

In this paper, we have investigated the excess entropy of a model fluid with $\phi(r)$, which possesses a soft repulsive core $\phi_0(r)$ and the long-range Friedel oscillations. At some specific density, the model fluid describes well the structural and dynamic properties of liquid Ga at $T = 323$ K. By simulation and the HS perturbation theory, we have calculated separately the excess entropy of the model fluid and that of the fluid with $\phi_0(r)$. For both models, the predictions of the HS perturbation theory agree well with the simulation results. By the difference between the excess entropies of the two model fluids, we obtain the contribution due to the Friedel oscillations. Indicated by our results, from low to high densities, the Friedel oscillations always cause a decrease in the excess entropy of the model fluid with $\phi(r)$ at $T = 323$ K.

Please cite this article in press as: K.H. Tsai, T.-M. Wu, Entropy of a model for liquid Ga: Contribution due to Friedel oscillations, Computer Physics Communications (2010), doi:10.1016/j.cpc.2010.07.014

Acknowledgements

T.M. Wu acknowledge financial support from National Science Council of Taiwan under No. NSC 97-2112-M-009-0005-MY2.

References

[1] K.H. Tsai, T.M. Wu, S.F. Tsay, T.J. Yang, J. Phys.: Condens. Matter 19 (2007) 205141.
[2] K.H. Tsai, T.M. Wu, S.F. Tsay, J. Chem. Phys. 132 (2010) 034502.
[3] J.P. Hensen, I.R. McDonald, Theory of Simple Liquids, Academic, New York, 1986.
[4] H. Kitamura, J. Phys.: Condens. Matter 19 (2007) 072102.
[5] C. Chandler, J.D. Weeks, H.C. Andersen, Science 220 (1983) 787.
[6] K.H. Tsai, T.M. Wu, J. Chem. Phys. 129 (2008) 024503.
[7] P.V. Giaquinta, G. Giunta, S.P. Giarritta, Phys. Rev. A 45 (1992) R6966.
[8] Z. Yan, S.V. Buldyrev, N. Giovambattista, H.E. Stanley, Phys. Rev. Lett. 95 (2005) 130604.
[9] D. Ben-Amotz, G. Stell, J. Chem. Phys. 120 (2004) 4844.
[10] J.R. Errington, T.M. Truskett, J. Mittal, J. Chem. Phys. 125 (2006) 244502.

Please cite this article in press as: K.H. Tsai, T.-M. Wu, Entropy of a model for liquid Ga: Contribution due to Friedel oscillations, Computer Physics Communications (2010), doi:10.1016/j.cpc.2010.07.014